Philippine Engineering Journal (1994) XV (2): 27-66

LIQUEFACTION-INDUCED LARGE GROUND DISPLACEMENTS: PART 2 - PREDICTION BY ENERGY MODEL

Rolando P. Orense, Dr. Eng.
Research Engineer
Kiso-jiban Consultants Co., Ltd.
Tokyo, Japan

ABSTRACT

This paper deals with the modeling of liquefaction-induced large permanent ground displacements. Based on the information obtained from case studies and shaking tables tests, a technique is developed to predict the ultimate ground displacements that will develop when the state of soil liquefaction is continued for a sufficiently long period of time. The method is based on principle of minimum potential energy, and effect of earthquake motion is removed from the analysis. The distribution of the ground displacement is derived so that the potential energy of the ground would take minimum value. Surface irregularity as well as ground heterogeneity are considered. Both two-dimensional and three-dimensional models are developed. Finally, the model is extended to include the temporal development of permanent displacement. This is done by solving the equation of motion where the transient displacement is expressed as a fraction of the ultimate one. An energy dissipation mechanism is incorporated stabilize the solution. Analyses made on both laboratory and actual field cases show the validity of the model. Thus, the technique can serve as an economical and practical tool to predict the potential seismic hazards to urban facilities and lifeline networks induced by the lateral flow of liquefied soil.

INTRODUCTION

In recent years, it has been recognized that lateral spreading induced by seismic liquefaction is among the most troublesome hazards for buried structures and lifeline facilities. The damage potential of lateral spreads is directly related to the order of magnitude of the permanent lateral ground displacements. Movements ranging between a few centimeters to several meters have been observed during past earthquakes.

The evaluation of permanent ground displacements is a difficult non-linear problem. However, it is important as the evaluation of the damaging effects of liquefaction at a site requires the ability to predict the magnitude and spatial distribution of permanent ground displacements. Even though the prediction if a site will liquefy or not can be done with reasonable degree of confidence, there is no generally accepted method for evaluating

displacements. Current research efforts are now focused on this subject.

Several techniques, ranging from simple empirical formulations to rigorous finite element procedures, have been developed by various researchers to predict permanent displacements of sloping grounds and earth structures. It may be useful to review these methods to present a clear view of the state of the art prediction.

A simple empirical equation for predicting liquefaction-induced displacements of one-dimensional slopes has been proposed by Hamada et al. (1986). This equation is based on measurements of ground displacements from aerial photographs taken before and after the earthquakes. Based on measurements of lateral displacements observed after the occurrence of earthquakes in a number of locations in western United States, Youd and Perkins (1987) developed the Liquefaction Severity Index (LSI) which is the maximum possible ground displacement that is expected to occur in a gently sloping Holocene fluvial deposits. From case history studies of liquefaction-induced lateral spread, Barlett and Youd (1992) developed an empirical model using multiple linear regression for predicting the amount of horizontal ground displacements at potentially liquefiable sites.

One of the earliest and probably the most widely used type of analysis is that proposed by Newmark (1965). The ground displacement is calculated based on a single degree of freedom system and rigid plastic soil. The earthquake load is represented by a pseudo-static load. When the earthquake-induced acceleration is less than a certain critical value, no sliding will occur; however, when the critical value is exceeded, permanent ground displacement will take place. The displacement is then derived by integrating the acceleration-time history in excess of the critical value. It should be noted that the above method, which has been adopted and modified by several researchers (e.g., Sarma, 1975; Franklin and Chang, 1977; Byrne, 1990; Baziar, 1991), is based on rigid-body movement of soil. When considering liquefied soil, however, the absence of a rigid soil makes the application of the model difficult. Moreover, the model, in its present form, can not account for the large strains and displacements that occur within the zone of liquefaction.

Lee (1974) proposed another type of analysis to determine the seismically-induced permanent deformation of earthfill dams. This method is based on the assumption that the deformation is due to the softening of the soil as a result of seismic shaking so that after the earthquake, the dam will deform to a new condition compatible with the new softened stiffness of the soil. The softened parameters are based on laboratory tests in which the in-situ stress conditions before and during the earthquake are simulated. Finite element analyses are then performed using the normal and reduced/softened moduli to calculate the earthquake-induced ground displacements. Similar method of analysis was used by Taniguchi et al. (1983) to predict the settlements of embankments during earthquakes. On the other hand, Kuwano and Ishihara (1988) adopted the model and employed triaxial torsion shear test apparatus to simulate static and dynamic loading.

A drawback of this method is that a large number of laboratory tests have to be performed in order to simulate as accurate as possible the in-situ stress state, which, in some instances, can be too complicated for any soil testing apparatus to simulate. Based on the fact that liquefied soil can undergo strains as large as 50 to 100%, the absence of available apparatus hinders the application of this model.

Much of the present available techniques in evaluating permanent displacements of earth structures employ non-linear dynamic stress-strain behavior of soil in conjunction with plasticity theory. These types of analyses include equivalent linear model (Seed et al., 1973; Lysmer et al., 1975), direct non-linear model (Finn et al., 1976; 1986) and elasto-plastic model (Dafalias and Hermann, 1982; Pastor and Zienkiewicz, 1986) among others. However, considering the fact that the analysis of liquefied soil requires highly non-linear analysis, too many input parameters have to be precisely determined in the laboratory. To compound the situation, the proper modeling of soil properties for analysis remains a formidable task.

It is apparent from the foregoing discussions that the methods of prediction are strongly related to the assumptions of the mechanisms by which ground displacements are governed. In this paper, an alternative model is presented which takes into account field experiences and shaking table observations, so that the method of prediction may be made as reasonable and brief as possible without sacrificing accuracy.

CHARACTERISTICS OF LIQUEFACTION-INDUCED GROUND DISPLACEMENTS

In a companion paper (Orense, 1994), the nature of permanent ground displacements of liquefied soil was clarified, and the factors influencing the magnitude and spatial distribution were identified based on a review of actual case histories and the results of shaking table tests. The characteristics of permanent ground displacements induced by liquefaction were summarized by the following observations:

1. The permanent displacement is oriented in the downward direction of a slope, suggesting the influence of gravity. Tension cracks are detected near the top of liquefied slopes in the field after movement, and they are oriented normal to the direction of the ground displacement.

2. Lateral displacements at the top of the slopes are greater than those at the foot of the slopes. In addition, subsidence is predominant near the top of the slope while heaving is the case in the lower portion. The magnitude of the vertical displacement is much smaller than that of the horizontal one.

3. Shaking table tests show that liquefied ground behaves very similar to liquid; hence, its movement is highly affected by the total head gradient which is defined in terms of the total overburden stress and the elevation heads.

4. The magnitude of the lateral displacement in a liquefied sandy layer is minimum at the bottom and increases towards the surface. When partially saturated layer at the surface is present, the lateral displacement is continuous at the interface between this layer and the underlying liquefied layer.

5. Permanent displacement is caused by the gravity force; cyclic acceleration influences the movement only indirectly by triggering liquefaction and in determining the extent of liquefaction.

6. The magnitude and pattern of ground movement depend not only on the slope and stratification local to the point of concern but on the overall topography of the study area.

The observations that liquefied soil behaves as liquid and that seismic forces affect displacements only indirectly are important since they imply that the effect of earthquake motion can be removed from the analysis, and the problem can be analyzed in a static manner. These observations, as well as the others mentioned above, will serve as the basis for the development of an analytical technique to predict liquefaction-induced permanent ground displacements, which will be presented in the next section.

2-D MODEL FOR PREDICTING PERMANENT GROUND DISPLACEMENTS

This section deals with an analytical model to predict the displacement of two-dimensional liquefied ground based on the principle of minimum potential energy. Before going into the formulation of the model, a brief review of the basic concepts of the energy principle will be presented.

Principle of Minimum Potential Energy

As discussed earlier, liquefied soil behaves as liquid. Consequently, its behavior can be analyzed and explained in terms of physical laws. One of the most commonly used principles in the analysis of structural and hydraulic phenomena is the principle of minimum potential energy. The principle is stated as follows (Washizu, 1968):
"Among all admissible configurations a system can undergo which satisfy the prescribed boundary conditions, the actual displacements make the total potential energy an absolute minimum"

Before applying the principle to the analysis of permanent ground displacements, it is worth illustrating the applicability of the concept to various physical phenomena.

Consider a block with weight W and attached to an initially unstretched elastic spring with modulus **k**, as shown in Figure 1. When the block is released from rest, it will oscillated and some of the energy are dissipated until the motion ceases.

The principle of minimum potential energy is employed to calculate the ultimate displacement **u** of the system. The change in the potential energy of the system, denoted by II consist of the change in the strain energy of the spring and the change in the potential energy of the mass, i.e.,

$$\Pi = \frac{1}{2}ku^2 - Wu \tag{1}$$

where **u** is the unknown displacement.

Minimizing the energy expression with respect to **u** and setting **t** to zero results in

$$\frac{\partial \Pi}{\partial u} = ku - W = 0 \qquad \text{or} \qquad u = \frac{W}{k} \tag{2}$$

which is equal to the exact solution.

Next, the displacement of water will be analyzed. Consider the U-tube shown in Figure 2. In the said tube, water in both pipes have different initial elevations. Now, assume that the valve connecting the pipes is suddenly opened. Water will flow until an equilibrium condition is reached. This equilibrium condition can be obtained by minimizing the energy function. Before the flow, the potential energy is given by

$$\Pi_o = \frac{1}{2}\gamma_w A \left\{H_1^2 + H_2^2\right\} \tag{3}$$

where A is the cross sectional area of the tube, γ_W is the unit weight of water and H_1, and H_2 are the elevations of the water in the pipes. When the valve is opened, the elevations of water inside the two pipes change to $H_1-\Delta H$ and $H_2+\Delta H$, where ΔH is the change in water elevation, and the potential energy becomes

$$\Pi_o+\Pi = \frac{1}{2}\gamma_w A \left\{(H_1 - \Delta H)^2 + (H_2 + \Delta H)^2\right\} \tag{4}$$

Thus, the change in potential energy is derived as

$$\Pi = \frac{1}{2}\gamma_w A \left\{(H_1 - \Delta H)^2 - H_1^2 + (H_2 + \Delta H)^2 - H_2^2\right\} \tag{5}$$

Proceeding as before,

$$\frac{\partial \Pi}{\partial(\Delta H)} = \frac{1}{2}\gamma_w A \{2(H_1 - \Delta H) - 2(H_2 + \Delta H)\} = 0 \tag{6}$$

whence, ΔH can be obtained as

$$\Delta H = \frac{H_1 - H_2}{2} \tag{7}$$

Therefore, the final elevation of water inside the tube is given by

$$H_1 - \Delta H = H_2 + \Delta H = \frac{H_2 + H_1}{2} \tag{8}$$

which shows that the water will move until the water levels on both sides of the tube are identical.

The examples shown above clearly illustrate the applicability of the principle of minimum potential energy in describing the movement of both solid and liquid. As shown above, motion ceases when equilibrium is achieved, which, in turn, corresponds to the point where energy is minimum. Thus, the principle can be used to predict the maximum possible displacement than can occur. It should be noted, however, that the principle is not concerned with how the material reaches this particular point; consequently, the principle can not be applied to predict the time history of displacement of the object concerned. The formulation of the temporal development of displacement will be presented later.

Model Formulation

The analytical model is derived from the observations on the nature and mechanism of soil flow described earlier. The most important of these is the observation that seismic motion affects ultimate displacements only indirectly by triggering liquefaction and in determining the extent of liquefaction. Consequently, the effect of seismic motion can be removed from the analysis and a static approach can be made by taking into account only the potential energy of the ground. It should be emphasized that the calculated displacement is the maximum possible that can occur when the state of soil liquefaction continues for a sufficiently long period of time.

The method employs the model ground shown in Figure 3. It consists of an unliquefiable base (B), a liquefiable layer (H) and a surface unsaturated layer (T). The surcharge, P, includes the weight of the unsaturated layer and any additional loading. The ground configuration varies linearly with the x-axis as follows:

$$\begin{aligned} B &= B_o + ax & H &= H_o + bx \\ T &= T_o + cx & P &= P_o + ex \end{aligned} \tag{9}$$

Four assumptions are employed in the analysis:

1. The lateral displacement **u** is approximated by a sinusoidal distribution along a vertical cross section (see Figure 4) as

$$u(x, z) = F(x) \sin \frac{\pi(z - B)}{2H} \tag{10}$$

where $F(x)$ is an unknown function of x and represents the displacement at the surface of the liquefied layer $(z=B+H)$.

2. Permanent displacement occurs under constant volume condition, i.e.,

$$\frac{\partial u}{\partial x}+\frac{\partial w}{\partial z}=0 \tag{11}$$

in which w(x,z) is the vertical displacement at any point. Note that the settlement resulting from consolidation is excluded and should be considered separately.

3. The stress-strain (τ-γ) relation of the liquefied sand is given by

$$\tau = G\frac{\partial u}{\partial z}+\tau_r \tag{12}$$

where G is the shear modulus and is τ the residual strength. Note that this relation combines both linear elastic and rigid plastic behaviors; this is adopted for analytical convenience.

4. The surface unsaturated layer does not liquefy and behaves as a solid bar with elastic modulus E.

Substituting Equation 10 into Equation 11 and considering zero vertical displacement at the base (z=B), the vertical displacement function w(x,z) is obtained as follows:

$$w(x,z) = -\frac{2}{\pi}\left[H\frac{dF}{dx}+bF\right]\left\{1-\cos\frac{\pi(z-B)}{2H}\right\}+\frac{aH+b(z-B)}{H}F\sin\frac{\pi(z-B)}{2H} \tag{13}$$

Specifically, at z=B+H, the vertical displacement at the surface of the liquefied layer is given by

$$w|_{z=B+H} = -\frac{2}{\pi}\left[H\frac{dF}{dx}+bF\right]+(a+b)F \tag{14}$$

Note that from the observation that there is no slip between the liquefied and surface unsaturated layers, Equation 14 is the vertical displacement of the ground surface as well. In addition, the change in surface elevation, δH, due to the lateral soil flow is derived from the difference of the flux of ground movement as shown in Figure 5 and is given by

$$\begin{aligned}\delta H &= \frac{\partial}{\partial x}(\text{Volume of soil flow})\\ &= \frac{2}{\pi}\left[H\frac{dF}{dx}+bF\right]\end{aligned} \tag{15}$$

The potential energy of the ground is then formulated by considering the strain and gravity components of the liquefied and surface unsaturated layers. The unliquefied base is stable and is not involved in the flow. In the calculation of the strain energy, only the predominant components of the strain tensor are taken into account. For the liquefied layer, a lateral surface displacement of 5 m is possible when the thickness of the liquefiable layer is, for example, 10 m, as in the case of Noshiro City (Hamada et al., 1986). This results in a shear strain of 50%. In contrast, the length of a slope is typically 500 m, and this gives an average normal strain of merely 1%. Moreover, the vertical displacement is much smaller than the lateral displacement, and consequently, the normal strain $\partial w/\partial z$, is also small. Since the strain energy is proportional to the square of the strain, the shear strain $\partial u/\partial z$ is the predominant component. The surface layer behaves like a column subjected to lateral compression and only the axial strain $\partial u/\partial x$ is important. Thus, the total energy consists of the following:

(1) Strain energy in the liquefied layer

$$E_1 = \int_0^L \int_B^{B+H} \left\{ \frac{G}{2} \left(\frac{\partial u}{\partial z} \right)^2 + \tau_r \frac{\partial u}{\partial z} \right\} dz dx \tag{16}$$

(2) Potential energy increment of the liquefied layer

$$E_2 = \int_0^L \frac{\gamma_l}{2} [(B + H + \delta H)^2 - (B + H)^2] \, dx \tag{17}$$

(3) Strain energy of the surface unsaturated layer

$$E_3 = \int_0^L \frac{ET}{2} \left(\frac{dF}{dx} \right)^2 dx \tag{18}$$

(4) Potential energy increment of the surcharge

$$E_4 = - \int_0^L P \times w|_{z=B+H} \, dx \tag{19}$$

Note that the integrand in Equation 17 is similar to Equation 5, the potential energy expression for water. Moreover, the potential energy is formulated by assuming that the soil material (with unit weight γ_l) remains in the space between $x=0$ and $x=L$, i.e., nothing is going into or out of the interval and no crack development. However, since liquefied soil can flow beyond this interval, a correction E_{bl} is required in order to take into account the increment in potential energy of the displaced volume of soil.

Figure 6 illustrates the condition at the foot of a slope $(x=0)$ where the displacement $F(x)$ is allowed to occur. To simplify the analysis, the potential energy of the volume of soil

ABE' is assumed to be equal to that of ABE (this is reasonable since the vertical displacement w is very small compared to the thickness of the liquefied layer AB) and this is given by

$$E_{b1}|_{x=0} = \int_B^{B+H} \gamma_l z\, F \sin\frac{\pi(z-B)}{2H}\, dz \Big|_{x=0}$$
$$= \gamma_l \left(\frac{2HB}{\pi} + \frac{4H^2}{\pi^2}\right) F \Big|_{x=0} \tag{20}$$

Similar calculation can be made at the top of the slope (x=L), and the potential energy of this volume of soil is subtracted from the total energy. Thus, the total correction can be written as

$$E_{b1}|_{x=0} + E_{b1}|_{x=L} = -\gamma_l \left(\frac{2HB}{\pi} + \frac{4H^2}{\pi^2}\right) F \Big|_{x=0}^{x=L} \tag{21}$$

Based on field observations, tension cracks can occur near the top of liquefied slopes. The presence of such cracks are incorporated by assuming that a crack is filled with sand-water mixture, as in Figure 7, which exerts lateral pressure on the side of the segment. For the purpose of the analysis, the case wherein lateral earth pressures are exerted at the top and bottom of the slope is considered. This pressure, consisting of hydrostatic and additional pressure due to surcharge, increases the potential energy at $x=0$ (negative work) and decreases at $x=L$ (positive work). Thus, the energy contribution is:

$$E_{b2} = \int_B^{B+H} \left\{ -[\,\gamma_l(B+H-z)+P\,] \times F \sin\frac{\pi(z-B)}{2H} \right\} dz \Big|_{x=0}^{x=L}$$
$$= -\left[\frac{2\gamma_l H^2}{\pi} + \frac{2PH}{\pi} - \gamma_l \left(\frac{2H}{\pi}\right)^2\right] F \Big|_{x=0}^{x=L} \tag{22}$$

Therefore the total potential energy of the ground, denoted by II, is given by

$$\Pi = E_1 + E_2 + E_3 + E_4 + (E_{b1} + E_{b2}|_{x=0} + (E_{b1} + E_{b2}|_{x=L} \tag{23}$$

which can be expressed as

$$\Pi = \int_0^L \mathcal{F}(x, F, \frac{dF}{dx})dx + \mathcal{G}(x, F)\Big|_{x=0}^{x=L}. \tag{24}$$

The above equation is then minimized to calculate the actual displacement F(x). This is a typical problem in variational calculus where the function F(x) is to be determined which makes the functional II minimum.

Close-Form Solution

According to the mathematical theory of variational calculus, Equation 24 can be minimized by employing Euler's differential equation, i.e.,

$$\frac{\partial \mathcal{F}}{\partial F} - \frac{d}{dx}\left[\frac{\partial \mathcal{F}}{\partial (dF/dx)}\right] = 0 \tag{25}$$

Upon substitution of the explicit expression of F into Equation 25, the following is obtained:

$$\frac{d}{dx}\left\{\left(\frac{4\gamma_l}{\pi^2}H^2 + ET\right)\frac{dF}{dx}\right\} - \frac{G\pi^2}{8H}F = \tau_r - (a+b)\left(P + \frac{2\gamma_l}{\pi}H\right) - \frac{2e}{\pi}H \tag{26}$$

By assuming that the liquefied sand behaves as liquid, G is set equal to zero. As a result, Equation 26 can be simplified into

$$\frac{dF}{dx} = \frac{C_4 x^2 + C_5 x + A_1}{C_1 x^2 + C_2 x + C_3} \tag{27}$$

where

$$\begin{aligned}
C_1 &= \frac{4\gamma_l b^2}{\pi^2} \\
C_2 &= \frac{8\gamma_l b H_o}{\pi^2} + Ec \\
C_3 &= \frac{4\gamma_l H_o^2}{\pi^2} + ET_o \\
C_4 &= -\frac{1}{2}\left\{(a+b)\left(e + \frac{2\gamma_l b}{\pi}\right) + \frac{2eb}{\pi}\right\} \\
C_5 &= \tau_r - (a+b)\left(P_o + \frac{2\gamma_l H_o}{\pi}\right) - \frac{2eH_o}{\pi}
\end{aligned} \tag{28}$$

and A_1 is parameter which takes into account the boundary condition. A closed-form solution to the above differential equation can be easily obtained from the appropriate boundary conditions.

Equation 27 is applicable only to one segment of ground undergoing permanent movement. However, the equation can be extended and applied to grounds with surface irregularities or varying properties by subdividing the ground into piece-wise linear segments. The potential energy of each segment is formulated independently, as given by Equation 23. By adding the energy of each segment is formulated independently, as given by Equation 23. By adding the energy terms corresponding to each segment, the total energy of the whole ground is derived. Using variational principle as before, it can be shown that the lateral displacement distribution $F(x)$ for each segment is given by Equation 27, where the constants of integration can be evaluated by considering displacement and stress continuities at the interfaces.

Thus, by subdividing the ground into piece-wise linear segments, surface irregularity and material variation are accounted for in the analysis. Equation 27 can be used to solve for the displacement distribution in each segment, subject to the appropriate boundary conditions as required by the variational principle. Hence, the problem simplifies into the solution of simultaneous linear equations in terms of F_i $(i=l, n)$, and a continuous function of $F(x)$ can be obtained for the whole liquefied ground.

Illustrative Examples

The model presented in the previous section is then employed to analyze various cases. Since it is difficult to make an accurate determination of soil properties at various locations, a common set is assumed for each analysis. In addition, it is assumed that the liquefied soil behaves as liquid, with $G = \tau_r = 0$.

The first analysis was made on the sloping ground of Mae Hill located in Noshiro City which liquefied during the 1983 Nihonkai-Chubu earthquake. The topography, which is subdivided into piece-wise linear segments as shown in Figure 8(a), is obtained from the study made by Hamada et al. (1986). In the application of the model, a fixed boundary is assumed at the bottom of slope where displacements are negligible and free boundary at the top of slope, where cracks are observed. Unit weights of 15.7 kN/m^3 and 17.6 kN/m^3 are assumed for the surface layer and liquefied layer, respectively. The Swedish weight sounding tests conducted in the area show an average value of $N_{sw} = 100$ in the surface unsaturated layer (Hamada et al., 1986). From the empirical formula proposed by Inada (1960) correlating the Swedish cone resistance value, N_{sw}, with the SPT N-value given by

$$N = 2 + 0.067 N_{sw} \tag{29}$$

an equivalent SPT blowcount of N=8 is obtained. Hence, the Young's modulus of the surface soil is estimated to be 10780 kN/m^2 by using the empirical equation proposed by Schultze and Menzenbach (1961):

$$E = 71 + 4.9N \quad (\text{kgf/cm}^2) \tag{30}$$

The observed displacements at the surface are shown in Figure 8(b), together with the calculated values. It is shown that the prediction slightly overestimates the measures values.

The second example deals with the result of shaking table test. For this purpose, the results of Model 6 test of the Public Works Research Institute (PWRI) (after Sasaki et al., 1991), is selected for the analysis. In this test, a gently sloped gravel surcharge was placed over one-half the length of the loose saturated deposit. The configuration of the model ground is shown in Figure 9(a). The unit weights are measures as 14.5 kN/m^3 for the surface layer and 19.6 kN/m^3 for the liquefied layer. The Young's modulus is estimated to be 98 kN/m^2. Shaking was then applied in four stages with the acceleration increasing in each subsequent stage.

For shaking table tests, a cracked boundary is not directly observed due to the fact that crack can not be maintained open as no sand flows into it (different from Figure 7); instead, due to the effect of the end wall, a series of crack opening and closing occurs. For practical purpose, this end is modeled as a fixed boundary.

The resulting deformation of the ground surface after the test is shown in Figure 9(b). Also plotted in the same figure are the calculated permanent displacements as denoted by the solid line. Note that the observed values are underestimated.

In order to improve the analysis, it is noted that the right portion of the displacement distribution shows negative dF/dx, indicting the existence of tensile stresses in the surface layer. Since sandy soil does not have tensile resistance, the problem is re-analyzed such that the E of the portion where dF/dx becomes negative is set to zero. In effect, the solution becomes iterative until the actual boundary of the portions under compression and tension is established. The improved estimates are shown by broken lines in Figure 9(b), and it is seen that the calculated values overestimate the measured data as intended. It is to be noted that in this test, the applied shaking (duration time of 20 seconds per shaking stage) was not long enough to attain the ultimate displacement, and therefore, overestimation is expected.

It is noted that in the case studies presented herein involving both actual field studies and shaking table tests, the predicted displacement tends to be an overestimation. Although the material properties employed in the analyses could be one of the reasons for this discrepancy, another reason seems that the present analysis is geared toward the calculation of maximum possible displacement. When the observed displacements are not the maximum possible displacements, overestimation is inevitable.

EXTENSION TO THREE-DIMENSIONAL CASE

The previous section discussed the development of a model to predict permanent displacements in a two-dimensional ground. However, considering that lifeline networks cover wide areas and are extensively spread, the prediction technique should be ultimately three-dimensional; otherwise, the analysis of the whole areas may be very costly. In this section, the three-dimensional extension of the energy model is presented.

Model Description

In the application of the model, the ground surface area is subdivided into several triangular finite elements as seen from the top; see Figure 10(a). A typical finite element

employed in the model is presented in Figure 10(b). Each element consists of the following layers in z-direction: (1) an unliquefiable base, with elevation B; (2) a liquefiable layer with thickness H; (3) a surface unsaturated layer with thickness T; and (4) the surcharge, P, which includes the weight of the surface layer and any additional loading. The ground configuration varies linearly with the x and y coordinates, i.e.,

$$\begin{aligned} B &= B_o + a_1 x + b_1 y \qquad H = H_o + a_2 x + b_2 y \\ T &= T_o + a_3 x + b_3 y \qquad P = P_o + a_4 x + b_4 y \end{aligned} \tag{31}$$

The constants B_o, a_1, b_1, H_o, .., a_4, b_4 can be determined from the known values of B, H, T and P at the nodal points.

For the three dimensional case, the lateral displacements in a vertical cross section of a liquefied ground in the directions of x and y-axes (denoted by u and v, respectively), are approximated by sinusoidal distributions in z-direction:

$$\begin{aligned} u(x,y,z) &= F(x,y)\sin\frac{\pi[z-(B_o+a_1x+b_1y)]}{2(H_o+a_2x+b_2y)} \\ v(x,y,z) &= J(x,y)\sin\frac{\pi[z-(B_o+a_1x+b_1y)]}{2(H_o+a_2x+b_2y)} \end{aligned} \tag{32}$$

The formulation for three-dimensional case is similar to the two-dimensional case presented earlier. In this case, however, the surface unsaturated layer behaves like an elastic plate which has an elastic modulus E and Poisson's ratio ν and is subjected to in-plane stresses. The constant volume condition is re-written as

$$\frac{\partial u}{\partial x} + \frac{\partial v}{\partial y} + \frac{\partial w}{\partial z} = 0 \tag{33}$$

and the surface displacement is obtained as follows:

$$\begin{aligned} w(x,y)|_{z=B+H} = \; & -\frac{2}{\pi}\left[H\left(\frac{\partial F}{\partial x}+\frac{\partial J}{\partial y}\right)+a_2F+b_2J\right] \\ & +(a_1+a_2)F+(b_1+b_2)J \end{aligned} \tag{34}$$

In addition, the change in surface elevation, H, at a given location (x,y) due to the lateral soil flow is derived from the difference of the flux of ground movement and is given by

$$\delta H = \frac{2}{\pi}\left[H\left(\frac{\partial F}{\partial x}+\frac{\partial J}{\partial z}\right)+a_2F+b_2J\right] \tag{35}$$

Note that $+\delta$H indicates heaving, while $-\delta$H suggests settlement.

Energy Consideration

The energy of each ground element is again formulated by considering the strain and gravity components of the liquefied and surface unsaturated layers as in the two-dimensional case. The total energy consists of the following:

1. Strain energy in the liquefied layer

$$E_1 = \int_B^{B+H} \left\{ \frac{G}{2} \left[\left(\frac{\partial u}{\partial z} \right)^2 + \left(\frac{\partial v}{\partial z} \right)^2 \right] + \tau_r \left[\frac{\partial u}{\partial z} + \frac{\partial v}{\partial z} \right] \right\} dz \tag{36}$$

2. Potential energy increment of the liquefied layer

$$E_2 = \frac{\gamma_l}{2} \left[(B + H + \delta H)^2 - (B + H)^2 \right] \tag{37}$$

3. Strain energy in the surface unsaturated layer

$$E_3 = \frac{ET}{2(1-\nu^2)} \left[\left(\frac{\partial F}{\partial x} \right)^2 + \left(\frac{\partial J}{\partial y} \right)^2 + 2\nu \left(\frac{\partial F}{\partial x} \frac{\partial J}{\partial y} \right) + \frac{1-\nu}{2} \left(\frac{\partial F}{\partial y} + \frac{\partial J}{\partial x} \right)^2 \right] \tag{38}$$

4. Potential energy increment of the surcharge

$$E_4 = -P \times w|_{z=B+H} \tag{39}$$

Equations 36 - 39 represent the energy components for a soil column located at coordinates *(x,y)*. To get the total energy of the element, the equations should be integrated throughout the area of the element, designated by *A*. Note that these expressions are essentially the three-dimensional extensions of Equations 16 - 19, which are the energy expressions for two-dimensional case.

The additional energy expressions at the boundaries are given by

$$E_{b1} = \int_S \int_B^{B+H} (\gamma_l \times \delta_n \times z)\, dz\, dS \tag{40}$$

$$E_{b2} = \int_L \int_B^{B+H} \left\{ \delta_n \times [\, P + \gamma_l (B + H - z)\,] \right\} dz\, dL \tag{41}$$

where δ_n is the component of the lateral displacement at any point normal to the element boundary, S is the perimeter of the element and L is the length of the appropriate side (cracked

boundary) of the element. The quantity inside the bracket in Equation 41 is the hydrostatic pressure distribution.

Therefore, the total potential energy in each element, represented by the functional II, is given by

$$\begin{aligned} \Pi &= \int_A (E_1 + E_2 + E_3 + E_4)\, dxdy + E_{b1} + E_{b2} \\ &= \int_A \mathcal{F}\left(x, y, F, J, \frac{\partial F}{\partial x}, \frac{\partial F}{\partial y}, \frac{\partial J}{\partial x}, \frac{\partial J}{\partial y}\right) dxdy + \int_S \mathcal{G}(x, y, F, J)\, dL \end{aligned} \tag{42}$$

From the above equations, it can be seen that II is a function of the unknown surface displacements *F(x,y), J(x,y),* their first-order derivatives, and the coordinates x and y. Thus, the problem is, in effect, reduced to a two-dimensional one involving only the surface lateral displacements. These unknown displacements can be calculated by applying variational principle on the functional II. Due to the complicated nature of the expressions involved, a closed-form solution is not attempted; instead, a two-dimensional *(x,y)* finite element-based formulation is employed.

Finite Element Formulation

In the finite element formulation, Rayleigh-Ritz method is employed by representing the surface displacements within an element by the linear interpolating functions

$$\begin{aligned} F(x, y) &= \alpha_1 + \alpha_2 x + \alpha_3 y \\ J(x, y) &= \beta_1 + \beta_2 x + \beta_3 y \end{aligned} \tag{43}$$

or, in terms of the unknown nodal displacements

$$\begin{aligned} F(x, y) &= N_1 F_1 + N_2 F_2 + N_3 F_3 \\ J(x, y) &= N_1 J_1 + N_2 J_2 + N_3 J_3 \end{aligned} \tag{44}$$

where N_1, N_2 and N_3 are the familiar shape functions which are expressed in terms of the coordinates x and y, while $F_1, \ldots, J_3$ are the unknown displacements at the nodes of the element. Note that the above interpolating function implies constant-strain condition within the element.

Equation 44 is then substituted into the energy functional II. For each element, II s a function simply of the nodal displacements F_i and J_i. The total energy of the whole system, which is equal to the sum of the energies of each individual element, is minimized by taking its variation with respect to the unknown nodal displacements F_i and J_i and setting it to zero, i.e.,

$$\delta \sum_{k=1}^{m} \Pi_k = \sum_{k=1}^{m} \frac{\partial \Pi_k}{\partial F_i} \delta F_i + \sum_{k=1}^{m} \frac{\partial \Pi_k}{\partial J_i} \delta J_i = 0 \tag{45}$$

where $i=1$ to n, n = number of nodal points, while $k=1$ to m, m = *number* of elements. The above equation can be solved by setting

$$\frac{\partial \Pi_k}{\partial F_i} = 0 \quad \text{and} \quad \frac{\partial \Pi_k}{\partial J_i} = 0 \tag{46}$$

Equations 46 represent 2n equations and, by rearranging these set of equations, they can be written in a more familiar form

$$\{P\} = [K]\{U\} \tag{47}$$

where **[K]** is the stiffness matrix and **{P}** is the equivalent load vector. Thus, the equation becomes a typical finite element problem where the displacement vector **{U}** is required.

In the application of the method, two boundary conditions are considered. Fixed ends correspond to boundaries where liquefaction does not occur or where displacements are negligibly small (usually at the bottom of slopes). On the other hand, cracks occurring on top of slopes are modeled as free boundaries, where Equations 40 and 41 are applicable.

It should be noted that tensile stresses may develop in the surface unsaturated layer as a result of the lateral movement of the ground. Since sandy soil cannot sustain tensile stresses, special consideration is needed in order to exclude the tensile behavior. The stresses which developed due to subsoil liquefaction as calculated from the above analysis are added to the average static stress in the surface soil given by

$$S_o = 1/2\, K_o \gamma_s T \tag{48}$$

where K_o is the coefficient of earth pressure at rest (assumed to be equal to 0.5 in this study), γ_s is the unit weight of the surface soil and T is the average thickness of the surface layer (evaluated at the center of the element). This total stress represents the actual stress in the surface layer during the liquefaction of the subsoil.

Elements which show tensile principal stresses are picked out and the elastic moduli in the direction indicated by the tension are reduced to one percent of the initial value. The original problem is then re-analyzed on the basis of the new, now anisotropic properties until "no tension" state is reached. To avoid unnecessarily large number of iterations, the computation is terminated when the percentage difference in the nodal displacements obtained in two successive iterations is less than ten percent. This criterion seems reasonable when compared with the required accuracy of permanent displacement prediction.

Illustrative Examples

To examine the capability of the proposed method, it is used to simulate the ground displacements observed in shaking table tests conducted at the Public Works Research Institute (PWRI) and those measured in Noshiro City during the 1983 Nihonkai-Chubu earthquake. Due

to the complexity involved in determining the soil parameters for case history studies, the present study again makes use of a common set of soil properties for each analysis. In addition, the liquefied soil is assumed to behave like liquid, with $G = 0$ and $\tau_r = 0$. For the surface unsaturated layer, $\nu = 0.30$ is used.

The first analysis considers the semi-circular liquefiable deposit of PWRI's Model 8 test (Sasaki et al., 1991). In this test, a semi-circular liquefiable deposit of 2 m in radius and 0.25 m in height was overlain by a cone-shaped graved embankment with radius of 1 m and a height of 0.15m at the center. This model ground was shaken in the longitudinal direction in three stages to determine the effect of the direction of excitation on the lateral movement. The relevant soil properties are as follows: $\gamma_t = 18.0$ kN/m^3, $\gamma_s = 13.3$ kN/m^3, and E = 294kN/m^2. Figure 11(a) shows the direction of ground flow after the first two stages. From this figure, it is noted that the surface of the semi cone-shaped embankment and the neighboring horizontal ground seem to move almost radially, i.e., in the direction of slope.

Figure 11(b), on the other hand, illustrates the spatial distribution of the ground displacement obtained by the proposed model. In the calculation, the nodal points along the circumference are assumed as fixed ends, whereas those located along the diameter are assumed to be fixed in the direction normal to the diameter and free in the direction parallel to the diameter. Although the calculated maximum displacement of 3.2 cm exceeds the maximum observed value of 2.7 cm, a comparison of the two figures reveals that the calculated distribution conforms with that obtained from the shaking table test and the ground displacements occurred in the radial directions.

Studies conducted by Hamada et al. (1986) revealed that permanent lateral displacements in the order of several meters occurred in Noshiro City after it was hit by an earthquake of magnitude 7.7. The permanent displacements in the city as measured from aerial photographs taken before and after the earthquake are shown in Figure 12. It is noted that the displacement are larger at high elevations while negligibly small at low places, and that the displacement vectors are directed downslope around the hilltop.

The proposed method is employed to simulate the observed displacements. The top of Mae Hill in the southern portion of the city, being surrounded by cracks, is replaced by a hollow space in the finite element model, and the cracks as free boundaries. Another free end is located in the north boundary of the element mesh for the southern portion along Highway Route No. 7, where cracks are also detected. On the other hand, fixed boundaries are assumed on lowland areas where the non-occurrence of liquefaction is observed. The soil profile is extrapolated from the cross-sections obtained by Hamada et al. (1986) and the soil properties employed are as follows: $\gamma_t = 17.6$kN/m^3, $\gamma_s = 15.7$kN/m^3, and E = 10780kN/m^2.

Figure 13 shows the calculated ground displacements, where the maximum permanent displacement calculated was 6.6 m. Hamada et al. (1986) observed that the maximum displacement in this area was approximately 5 m. It can be seen that although the analysis slightly overestimates, the method shows good agreement with the measured data. Moreover, the spatial distributions are also consistent with those observed, i.e., displacements are large at high elevations and small at low elevations.

Since the liquefied soil is assumed to behave like liquid with zero residual strength, the calculated displacements can be considered as the upper-bound solutions, i.e., these displacements are the maximum possible displacements that would occur if soil liquefaction continues for a sufficient period of time.

It is noted that the proposed method, being static in nature, does not require complicated soil properties as input data. Information on topography, location of liquefied layer, unit weight of the soil, and the elastic properties of the surface unsaturated layer are the only required parameters. The heterogeneity of the ground can be considered by allowing different values of soil properties to various elements, it necessary. Surface irregularity can be taken into account by varying the thickness of the appropriate layers. Furthermore, since the liquefiable layer and surface unsaturated layer are assumed as elastic material and liquid, respectively, the computation is relatively straight forward and is not time consuming. For example, the analysis of Noshiro City, wherein the area was divided into 314 finite elements, took only 6 minutes of CPU time per iteration in an ordinary personal computer.

TEMPORAL DEVELOPMENT OF PERMANENT DISPLACEMENTS

The previous sections have discussed the ultimate displacement that could possibly occur when a liquefied ground is allowed to flow for a sufficiently long time. Generally, the ground displacement caused by earthquakes of large magnitude (probably greater than 7) seem to be close to the predicted one because the duration time of ground shaking is long enough. However, when an earthquake of smaller magnitude occurs at a shallow depth beneath the study area, it is possible that the ground shaking would be strong enough to trigger liquefaction but the resulting short duration may induce displacements smaller than the ultimate values. Thus, it is attempted to take into consideration the development of ground displacement with time. The formulation is made as simple as possible, like the original model, without sacrificing its reliability.

Theory of Dynamic Analysis

As shown in the previous sections, the prediction of the ultimate displacement was made by employing variational principle. Similarly, the temporal solution of displacement is derived by solving the Lagrangian equation of motion which is also a variational principle of dynamic type.

For convenience of analysis, the effect of time t on the ultimate displacements u and w are separately considered, i.e.,

$$\begin{aligned} U(x,z,t) &= \lambda(t)\, u(x,z) \\ W(x,z,t) &= \lambda(t)\, w(x,z) \end{aligned} \tag{49}$$

in which $\lambda(t)$ is function of time that varies from zero at the initial stage of shaking up to unity after a sufficiently long time. The expressions for u(x,z) and w(x,z) have already been obtained, and only $\lambda(t)$ is to be determined.

The Lagrangian equation of motion is given by

$$\frac{d}{dt}\left[\frac{\partial}{\partial\lambda}(\Gamma - \Pi)\right] - \frac{\partial}{\partial\lambda}(\Gamma - \Pi)) = \Psi \tag{50}$$

where λ is called the generalized displacement function with its time derivative dqenoted by , Γ and II refer to the kinematic energy and potential energy, respectively. Note that II consists of the contribution of the strain energy and gravity. Ψ on the right-hand side is the inertia force due to shaking. In the present case, when a potential function Υ exists, the force can be expressed as

$$\Psi = -\frac{\partial\Upsilon}{\partial\lambda} \tag{51}$$

By using Equation 51 and choosing λ (t) in Equation 49 as the generalized displacement in Equation 50, the Lagrangian equation of motion becomes

$$\frac{d}{dt}\left[\frac{\partial}{\partial\dot{\lambda}}(\Gamma - \Pi - \Upsilon)\right] - \frac{\partial}{\partial\lambda}(\Gamma - \Pi - \Upsilon) = 0 \tag{52}$$

The kinematic energy, Γ, is given by

$$\Gamma = \int_V \frac{\rho}{2}\left[\left(\frac{\partial U}{\partial t}\right)^2 + \left(\frac{\partial W}{\partial t}\right)^2\right] \, dV \tag{53}$$

where ρ is the mass density of the soil and the volumetric integration is made all over the liquefied and surface unsaturated layers where the displacement takes place. Substitution of Equation 49 into Equation 53 results in

$$\begin{aligned} \Gamma &= \frac{1}{2}\int_V \rho\left(u^2 + w^2\right) \, dV \, \left(\frac{d\lambda}{dt}\right)^2 \\ &= \frac{1}{2} m \left(\frac{d\lambda}{dt}\right)^2 \end{aligned} \tag{54}$$

where m denotes the quantity inside the integration sign. The potential energy, II, at the ultimate condition (i.e., $U = u$ and $W = w$) has been calculated earlier (see Equation 23). Substituting Equation 49 into II in place of **u** and **w** results in

$$\Pi = \frac{1}{2}k\lambda^2 + f\lambda \tag{55}$$

in which

$$\begin{aligned} k &= \int_0^L \left[ET\left(\frac{dF}{dx}\right)^2 + \frac{4\gamma}{\pi^2}\left(\frac{d(HF)}{dx}\right)^2\right] dx \\ f &= -k \end{aligned} \tag{56}$$

Neglecting the component of the inertia force in the vertical direction, the potential function of the inertia force is given by

$$\begin{aligned} \Upsilon &= -\int_V \Psi\, U\, dV \\ &= \int_V \rho \frac{d^2 u_b}{dt^2} U\, dV \end{aligned} \tag{57}$$

where d^2u_b/dt^2 indicates the seismic acceleration at the base of the liquefied layer. When Equation 49 is substituted into Equation 57,

$$\Upsilon = n \frac{d^2 u_b}{dt^2} \lambda \tag{58}$$

in which

$$n = \int_V \rho\, u\, dV \tag{59}$$

Upon substitution of Equations 51, 54, 55, and 58 into Equation 50, the Lagrangian equation of motion is transformed into

$$m\frac{d^2\lambda}{dt^2} + k\lambda = -f - n\frac{d^2 u_b}{dt^2} \tag{60}$$

Now, considering a base motion which is a harmonic function of time, i.e.,

$$\frac{d^2 u_b}{dt^2} = A \sin \omega t \tag{61}$$

Equation 60 becomes

$$m\frac{d^2\lambda}{dt^2} + k\lambda = -f - nA \sin \omega t \tag{62}$$

which can be easily solved analytically.

It should be mentioned at this point that the formulation presented herein assumes no temporal change in the thickness of the liquefied layer. On the other, the studies made on shaking table tests presented earlier concerning the ultimate displacements u and w were observed after pore pressure dissipation. Therefore, the present analysis takes into account implicitly the effect of pore pressure dissipation. An analysis incorporating explicitly the effects of pore pressure dissipation and reconsolidation of the ground was not attempted.

Mechanism of Energy Dissipation

When the equation of motion given by Equation 62 is applied to analyze the behavior of model grounds, two problems were observed: first, the predicted displacement developed much more rapidly than that observed in shaking table tests; and second, the predicted displacements oscillated around the ultimate one without decay of amplitude. Apparently, these problems stem from the lack of any energy dissipation mechanism in Equation 62. Therefore, an appropriate energy dissipation mechanism is proposed.

The mechanism of energy loss is developed by observing the behavior of liquefied sand during the shaking table test. Figure 14 illustrates the configuration of a model ground shaken at PWRI. The location of various transducers are also shown in the figure.

Figure 15 illustrates the relationship between the horizontal acceleration (A-18) in the liquefied layer and the lateral displacement at the surface (D-6) relative to the shaking table. The equation of motion indicates that this acceleration is more or less proportional to the shear stress, while the displacement gives a rough evaluation of the shear strain in the model ground. Hence, Figure 15 can be used to examine the stress-strain behavior of the liquefied soil. Except in the first few cycles, it is seen that the liquefied sand exhibited a temporary shear stiffness and did not behave similar to liquid, contrary to the idea mentioned before. For a certain period after unloading of shear stress from its peak values at A and C, the shear stress and tangent modulus are very small and the sand can undergo significant amount of deformation. After a substantial displacement in both directions, the shear stress starts to develop and this increase in shear stress prevents further movement of the ground. Following the peak shear stress attained at C and A', the phase of unloading and reloading in the other direction is accompanied again by the rapid development of shear distortion. Thus, a liquefied ground flows toward the location of the minimum potential energy as discussed earlier, and the movement is associated with the temporal development and disappearance of shear resistance of sand.

The variation of lateral movement in the manner of development as described above is closely related to dilatancy in ground, which either increases or decreases the excess pore water pressure and thereby affects the resistance of sand against shear distortion. This can be seen clearly in Figure 16, which shows the relationship between the pore water pressure and shear stress as estimated from the ground acceleration. It is seen that the excess pore water pressure drops significantly at the instant the peak shear stress is attained, such as in A and C; this is more pronounced in C in the positive direction. This behavior of water saturated sand is commonly observed in undrained shear tests. Conversely, the pore water pressure increases again after the peak stress, and is maintained at high value until the next peak stress is approached. Therefore, it is reasonable to say that the high level of excess pore water pressure allows the liquefied sand to deform without significant resistance against shear except after the shear distortion has occurred substantially in each half cycle of shaking and the peak shear stress is approached.

Although the soil behavior as summarized above should be modelled precisely for the purpose of dynamic analysis, this type of approach requires a step-by-step or an iterative integration of the equation of motion. This is because the change in the deformability of sand is related to either the shear distortion (Figure 15) or the ground acceleration (Figure 16), both of which are not known until the equation is solved. Thus, the computation becomes much more complicated than a closed-form solution which is the goal of the present study.

In order to simplify the analysis, Figure 17, which illustrates the relationship between the base acceleration or inertia forcer (A-26) and the ground displacement (D-6) as obtained from the PWRI experiment, is employed. Initially, the ground displacement can occur freely after the peaks of the inertia force, A and C. This phase corresponds to the stage after the peak shear stress when the excess pore water pressure of high as shown in Figure 16. The rate of development of displacement decreases gradually in the following stage, until the peak inertia force occurs and the nearly vertical gradient of the curve at peaks suggests a very limited possibility of continued flow of the ground.

To model the ground behavior as discussed above, a liquefied ground is allowed to move in accordance with Equation 62 without viscosity from the moment of peak inertia force (A and C in Figure 17) to the moment of null inertia force (B and D). At B and D, the ground movement is ceased abruptly and no more displacement is allowed until the next peak inertia force occurs at C and A'. This implies that a repeated loading and unloading is necessary, however small its magnitude may be, in order to keep the ground moving laterally. In other words, the ground will continue to move as long as shaking is occurring with low level of amplitude.

Therefore, Equation 62 is solved with the idea illustrated by Figure 17. The value of λ at the end of each cycle of inertia loading, denoted by λ_i, is given by

$$\lambda_i - 1 = (\lambda_{i-1} - 1)\cos\left(\frac{\pi\sqrt{k/m}}{2\omega}\right) + \frac{nA}{m\omega^2 - k}\left[\cos\left(\frac{\pi\sqrt{k/m}}{2\omega}\right) - \cos^2\left(\frac{\pi\sqrt{k/m}}{2\omega}\right)\right] \qquad (63)$$

which is easy to calculate with the initial condition $\lambda_0=0$ at the beginning of shaking and liquefaction.

Example Calculation

To illustrate the validity of the model, the development of λ with time as observed in small-scale shaking table test is simulated. The configuration of the model ground is illustrated in Figure 18. The loose deposit of sand was created in the container by jetting pressurized water into a sand deposit. The relative density of the ground was 38%. the model ground was shaken horizontally with an acceleration amplitude of 200 gals and a frequency of 5 Hz. Shaking was continued for a sufficiently long period of time until the ultimate displacements, u and w, were obtained. The movement of the targets placed on the ground surface was recorded by a videoY camera to obtain the experimental value of λ defined as the ratio of the displacement of the target at any time to the ultimate displacement.

Figure 19 compares the experimental λ of the model ground and the calculated value using the model. It can be seen that the agreement is satisfactory. It should be noted that the model requires limited number of input data such as the unit weight of soil, elastic modulus of the surface unsaturated layer (if any), and the ground configuration. Dynamic soil properties are not required because they are already taken into account in the dilatancy modeling.

To test the validity of the model in predicting the temporal development of displacement in actual scale, it is employed to simulate the behavior of a 400 m long ground in which the thickness of the liquefiable layer is 5 m throughout and is overlaid by a 1 m thick surface unsaturated layer. The slope of the ground is 1%. The unit weight of the liquefied soil is 17.6 kN/m^3 while that of the surface layer is 15.7 kN/m^3. The elastic modulus of the surface layer is 10780 kN/m^2. The foot of the slope is considered fixed, while an open crack is assumed at the top of the slope. Prior analysis showed that the ultimate displacement is maximum at the top of slope, with the value equal to 5 m.

The dynamic analysis illustrated in Figure 20 shows that as much as 3000 seconds of shaking is needed for the loading and unloading of the inertia force to occur so that the displacement can develop to the ultimate magnitude. Apparently, the main shaking of an earthquake does not last for this long period of time, although the state of liquefaction and the high pore water pressure can continue for several minutes. However, it is possible that there are other sources of ground shaking which is responsible for movement of the liquefied ground. Firstly, the main shaking of major earthquakes is accompanied by a "coda" wave and a minor excitation can keep the ground shaking for a longer time. As this continues, the loading and reloading of the inertia force is repeated and the ground displacement can continue further. Secondly, the lateral movement of the ground can in turn be the cause of self-generated shaking, as suggested by an observation of dynamic pore pressure fluctuation in rapidly shearing granular material (Iverson and LaHusen, 1989).

CONCLUSION

Based on the observations derived from case histories and shaking table tests, an analytical technique was developed to predict the ultimate ground displacements induced by liquefaction. The technique of calculation can be summarized as follows:

1. The method is based on the principle of minimum potential energy, and the effect of earthquake motion is removed from the analysis.

2. The model is concerned with the ground displacements that will develop when the state of soil liquefaction is continued for a sufficiently long period of time. Thus, the calculated displacement represents the maximum possible one.

3. Liquefied soil is assumed to behave like liquid. Lateral displacements are approximated by sinusoidal distribution along a vertical section and the vertical displacements are calculated based on constant volume condition.

4. The variation of permanent ground displacement with time can be incorporated into the model by considering the Lagrangian equation of motion. An energy mechanism model which is related to the dilatancy of the ground is introduced to stabilized the solution.

5. Analyses made on both laboratory and actual field cases showed good correlation with observed displacements.

Inspite of its simplicity, the example calculations made on both experimental and field conditions proved the validity of the model. Hence, the proposed method can serve as a practical

and economical tool to predict the potential seismic hazards to urban facilities and lifeline networks induced by the lateral flow of liquefied soil.

AKNOWLEDGMENTS

The majority of the work presented in this paper formed part of the thesis of the author for the Doctor of Engineering degree presented in 1992. As such, acknowledgments are due to all people who actively helped. Particular acknowledgments are due to Prof. Ikuo Towhata of University of Tokyo who supervised the research at that time. Thanks are also due to the Association for the Development of Earthquake Prediction (ADEP) and the Public Works Research Institute (PWRI) for the data provided to the author. The financial support provided by the Ministry of Education, Science and Culture (Monbusho) of the Japanese Government is gratefully acknowledged.

REFERENCES

Bartlett, S.F. and Youd, T.L. (1992). "Empirical Prediction of Lateral Spread Displacement," Proceedings, 4th Japan-US Workshop on Earthquake-Resistant Design of Lifeline Facilities and Countermeasures for Soil Liquefaction, Hawaii, 351-365.

Baziar, M.H. (1991). "Engineering Evaluation of Permanent Ground Deformations due to Seismically-Induced Liquefaction," PhD Thesis, Rensselaer Polytechnic Institute, Troy, New York.

Byrne, P.M. (1990). "A Model for Predicting Liquefaction-Induced Displacements," Soil Mechanics Series No. 147, Dept. of Civil Engineering, University of British Columbia, Vancouver, B.C.

Dafalias, Y.F. and Hermann, L.R. (1982)). "Bounding Surface Formulation of Soil Plasticity," Soil Mechanics - Transient and Cyclic Loads, Pande, G. and Zienkiewicz, O.C., Eds., John Wiley and Sons, Inc., London, U.K., 253-282.

Finn, W.D.L., Lee, W.K. and Martin, G.R. (1976). "An Effective Stress Model for Liquefaction," Journal of Geotechnical Engineering Division, ASCE, Vol. 103, GT6, 517-533.

Finn, W.D.L., Yogendrakumar, M. Yoshida, N. and Yoshida, H. (1986). "TARA-3:A Program to Compute the Response of 2-D Embankments and Soil-Structure Interaction Systems to Seismic Loadings," Department of Civil Engineering, University of British Columbia, Vancouver, Canada.

Franklin, A.G. and Chang, F.K. (1977). "Permanent Displacements of Earth Embankments by Newmark Sliding Block Analysis," U.S. Army Engineer Waterways Experiment Station Miscellaneous Paper S-71-17.

Hamada, M., Yasuda, S., Isoyama, R. and Emoto, K.(1986). Study on Liquefaction Induced Permanent Ground Displacements. Report of the Association for the Development of Earthquake Prediction (ADEP), Tokyo.

Inada, M. (1960). "Use of the Swedish Type Sounding Test Results," Tsuchi-to-Kiso, Vol. 8, No. 1, 13-18 (in Japanese).

Iverson, R.M. and LaHusen, R.G. (1989). "Dynamic Pore Pressures Fluctuations in Rapidly Shearing Granular Materials," Science, Vol. 246, 796-799.

Kuwano, J. and Ishihara, K. (1988). "Analysis of Permanent Deformation of Earth Dams due to Earthquakes," Soils and Foundations, Vol. 28, No. 1, 41-55.

Lee, K.L. (1974). Seismic Permanent Deformations in Earth Dams," Report to National Science Foundation, Project G138521.

Lysmer, J., Udaka, T., Tsai,C.F. and Seed, H.B. (1975). "FLUSH: A Computer Program for Approximate 3-D Analysis of Soil-Structure Interaction Problems," Report No. EERC 75-30, Earthquake Engineering Research Center, University of California, Berkeley.

Newmark, N.M. (1965). "Effects of Earthquakes on Dams and Embankments," Geotechnique, Vol. 5, No. 2, 137-160.

Pastor, M. and Zienkiewicz, O.C. (1986). "A Generalized Plasticity, Hierarchical Model for Sand Under Monotonic and Cyclic Loading," Proceedings, 2nd International Symposium on Numerical Models in Geomechanics, Ghent, 131-150.

Sarma, S.K. (1975). "Seismic Stability of Earth Dams and Embankments," Geotechnique, Vol. 25, No. 4, 126-132.

Sasaki, Y., Tokida, K., Matsumoto, H., and Saya, S. (1991). "Experimental Study on Lateral Flow of Ground due to Soil Liquefaction," Proceedings, 2nd International Conference on Recent Advances in Geotechnical Earthquake Engineering and Soil Dynamics, St. Louis, Missouri, 263-270.

Schultze, E. and Menzenbach, E. (1961). "Standard Penetration Test and Compressibility of Soils," Proceedings, 5th International Conference on Soil Mechanics and Foundation Engineering, Paris, Vol. 1, 527-532.

Seed, H.B., Lee, K.L., Idriss, I.M., and Makdisi, F. (1973). "Analysis of the Slides in the San Fernando Dams During the Earthquake of February 9, 1971," Report EERC 73-2, Earthquake Engineering Research Center, University of California, Berkeley.

Taniguchi, E., Whitman, R.V. and Marr, W.A. (1983). "Prediction of Earthquake-Induced Deformation of Earth Dams," Soils and Foundations, Vol. 23, No. 4, 126-132.

Washizu, K. (1968). Variational Methods in Elasticity and Plasticity, 3rd Ed., Pergamon Press, England.

Youd, T.L. and Perkins, D.M. (1987). "Mapping of Liquefaction Severity Index," Journal of Geotechnical Engineering Division, ASCE, Vol. 113, GT11, 1374-1391.

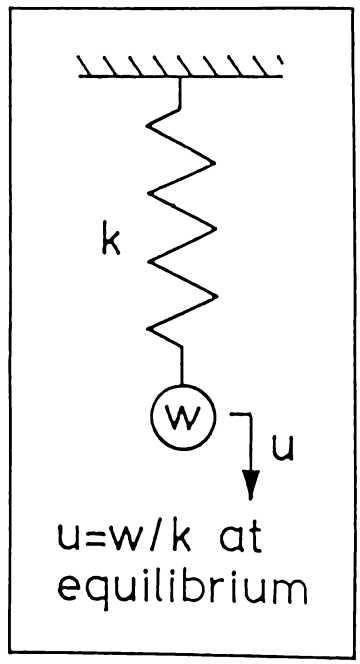

Figure 1: Spring-mass system

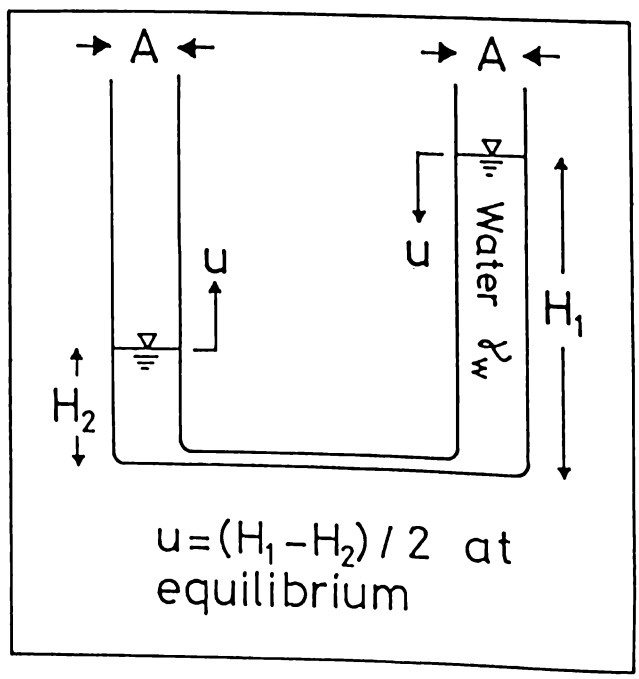

Figure 2: Flow of water in U-tube

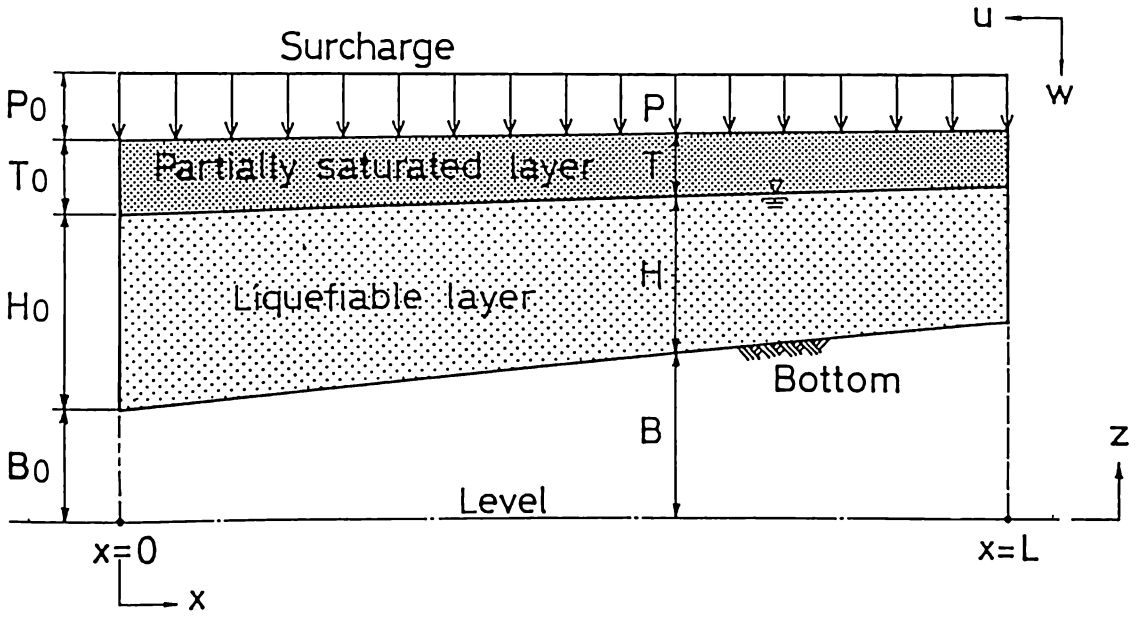

Figure 3: Model of Liquefied ground

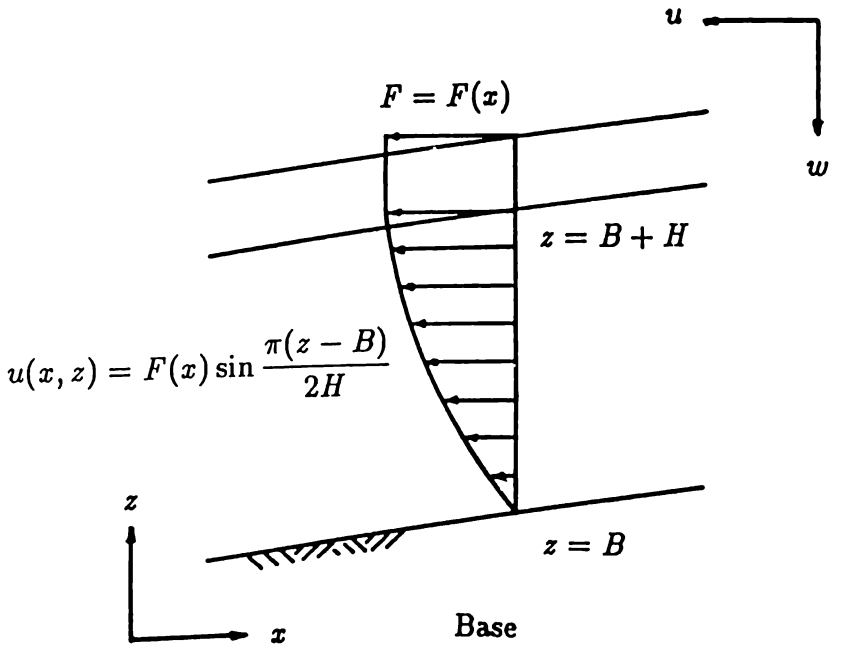

Figure 4: Lateral displacement distribution

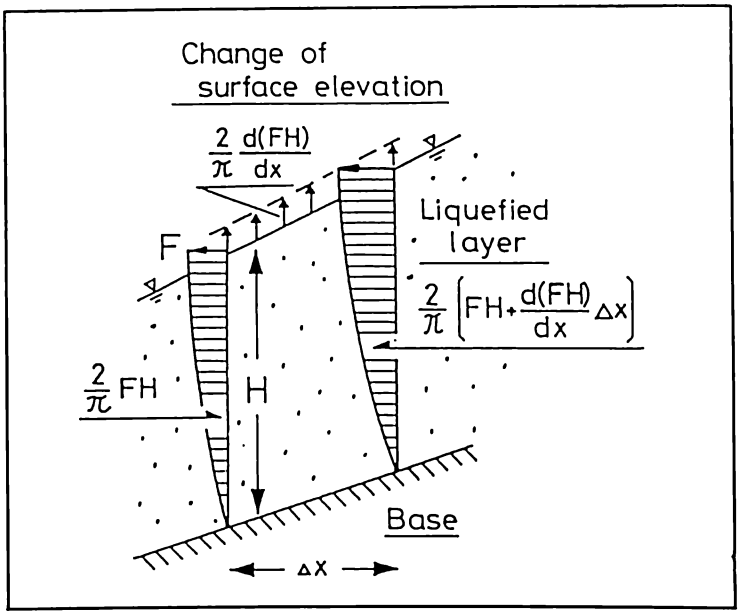

Figure 5: Volume flux of ground movement

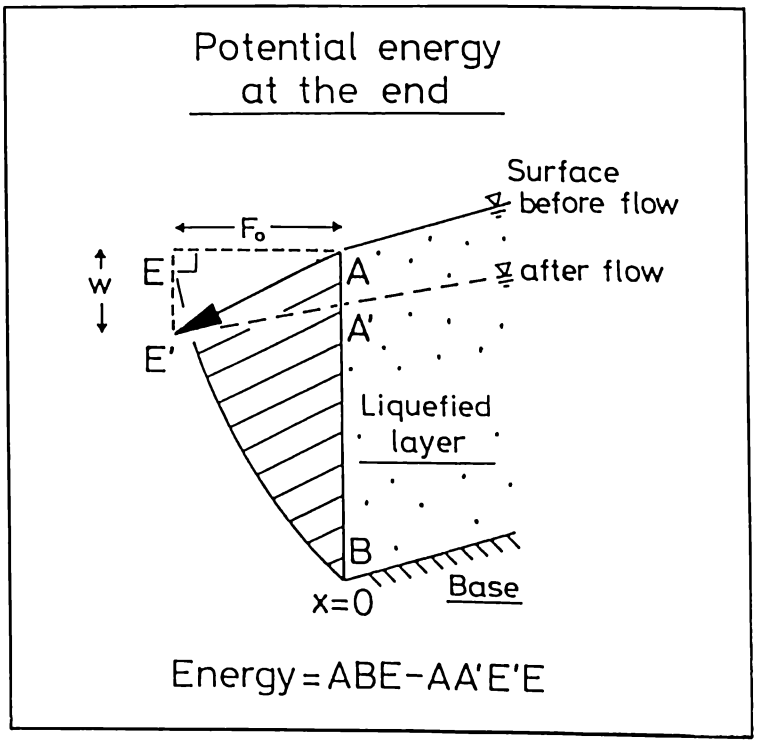

Figure 6: Potential energy at the boundary

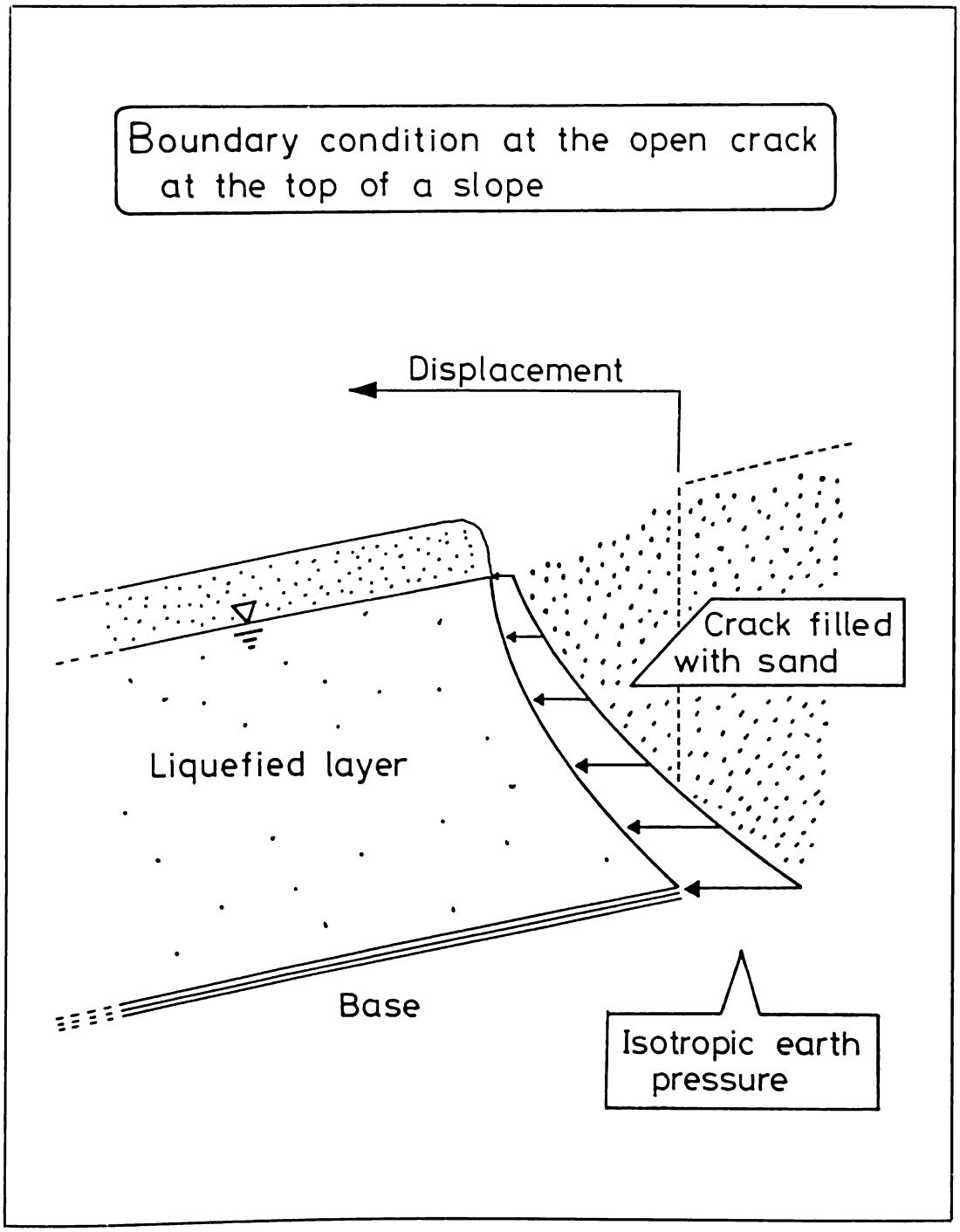

Figure 7: Model of free boundary with crack filled with water-sand mixture

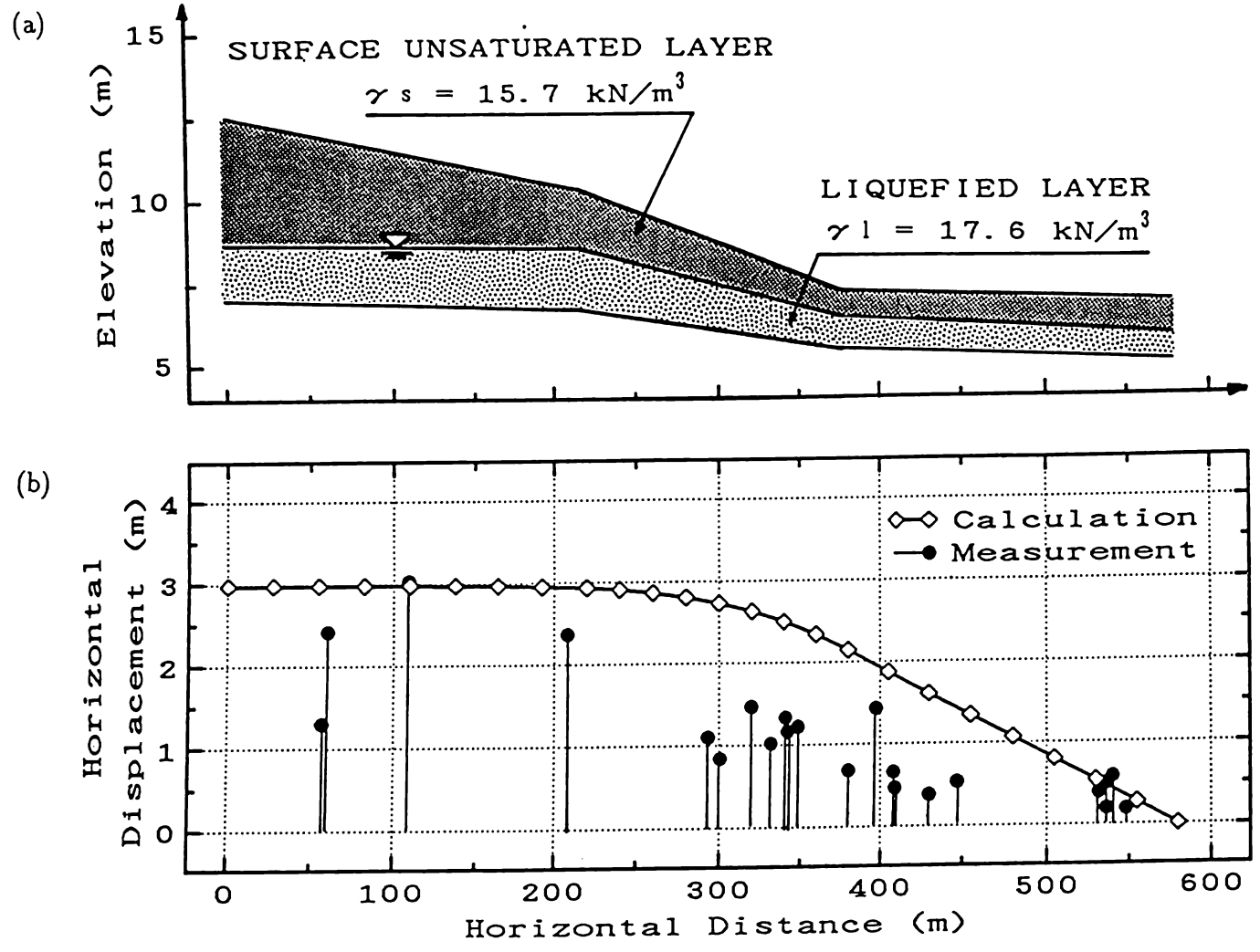

Figure 8: Case history analysis of Noshiro City: (a) soil profile; (b) observed and calculated permanent ground displacements

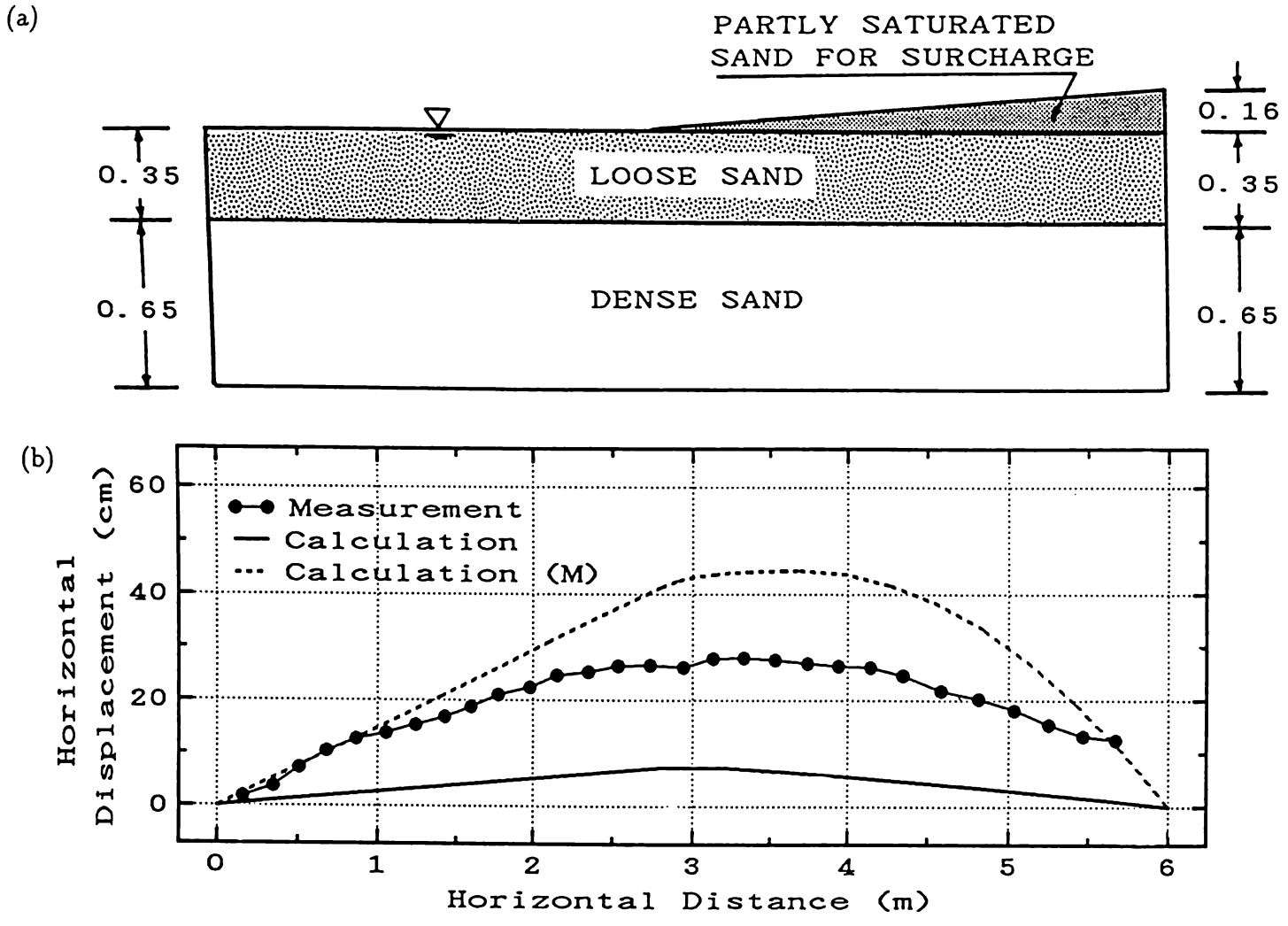

Figure 9: Model 6 test of PWRI: (a) model ground; (b) observed and calculated permanent ground displacements

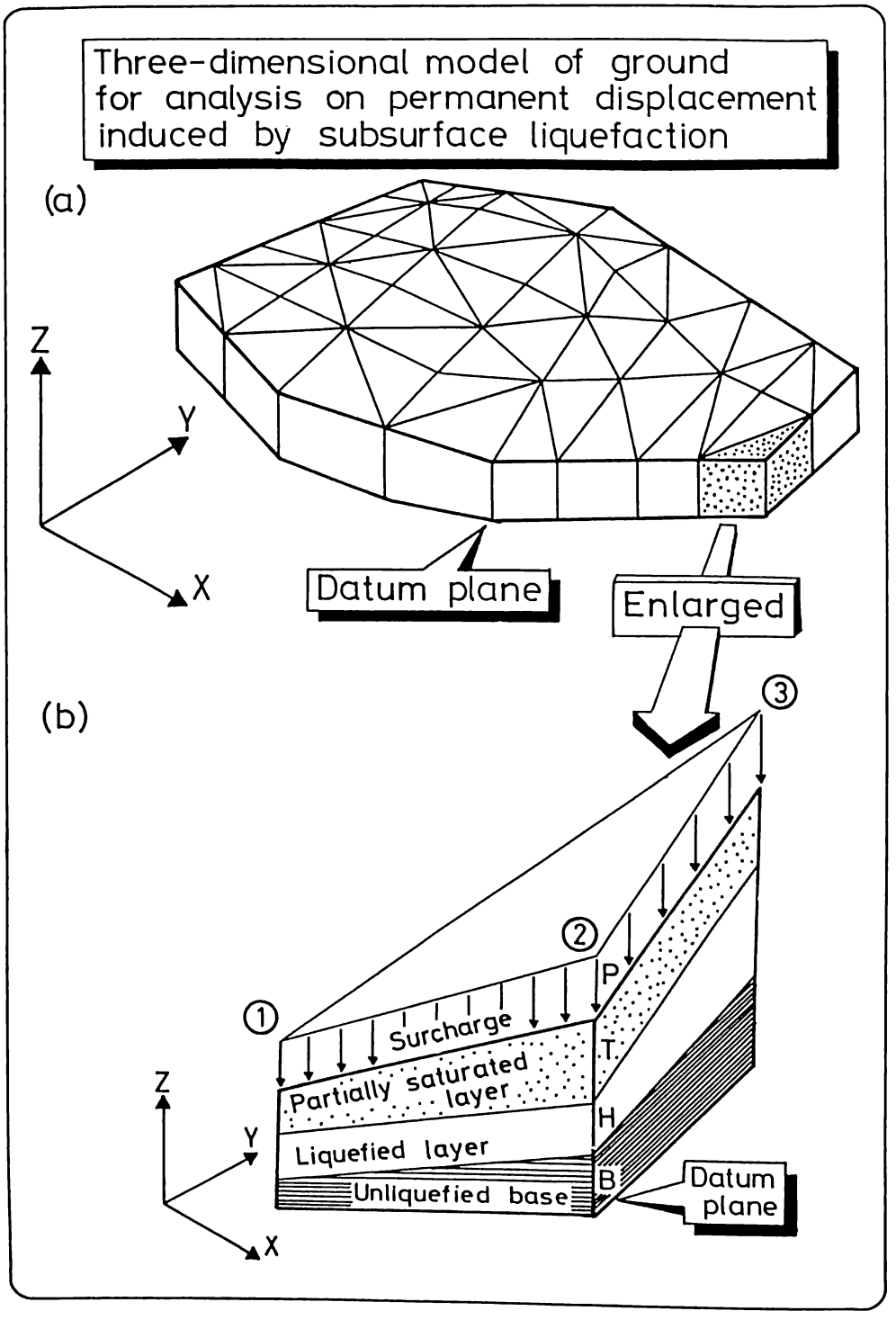

Figure 10: (a) Finite element mesh; (b) A typical finite element of the model ground

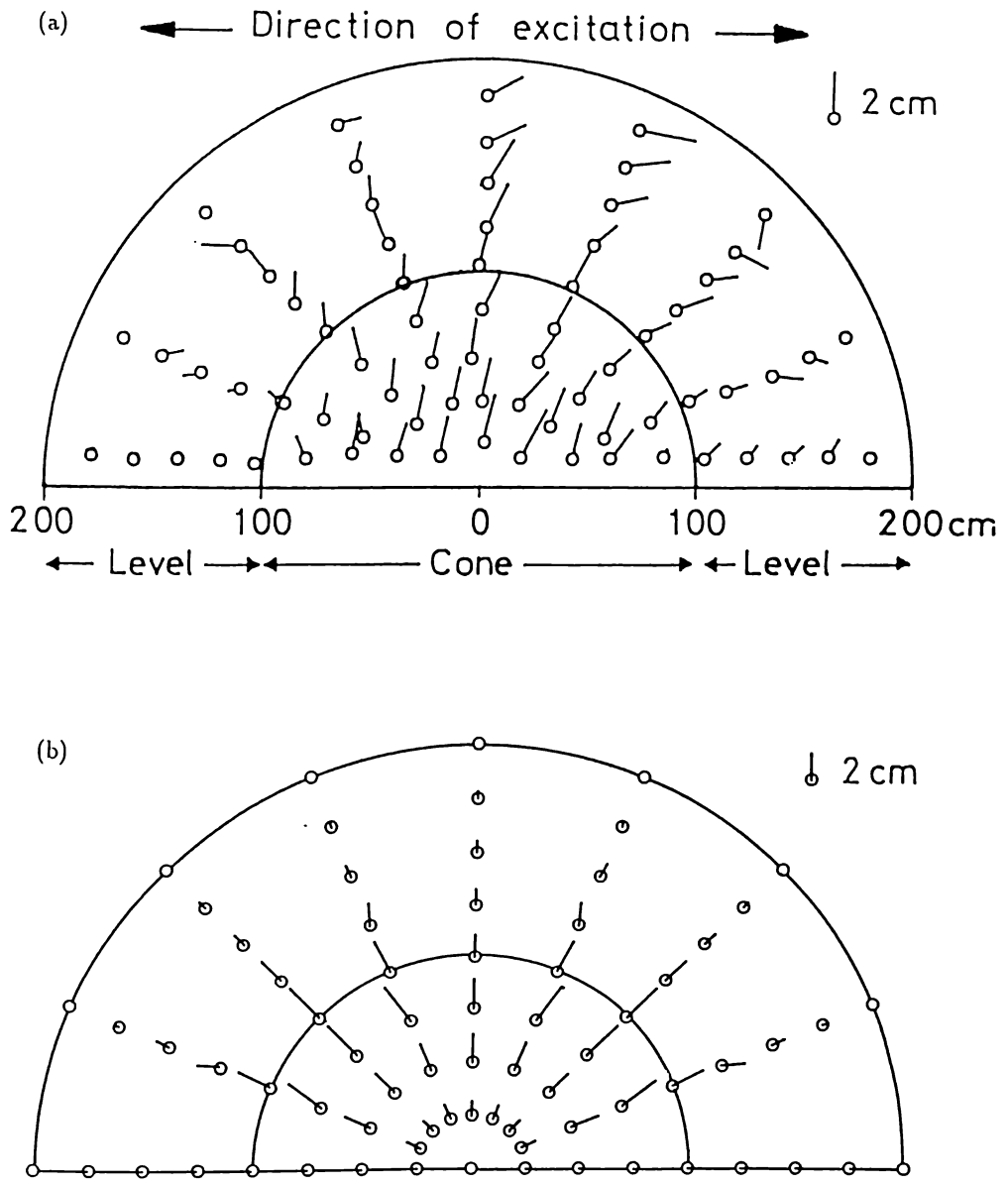

Figure 11: Model 8 test of PWRI: (a) observed direction of ground flow (after Sasaki et al., 1991); (b) calculated permanent ground displacements

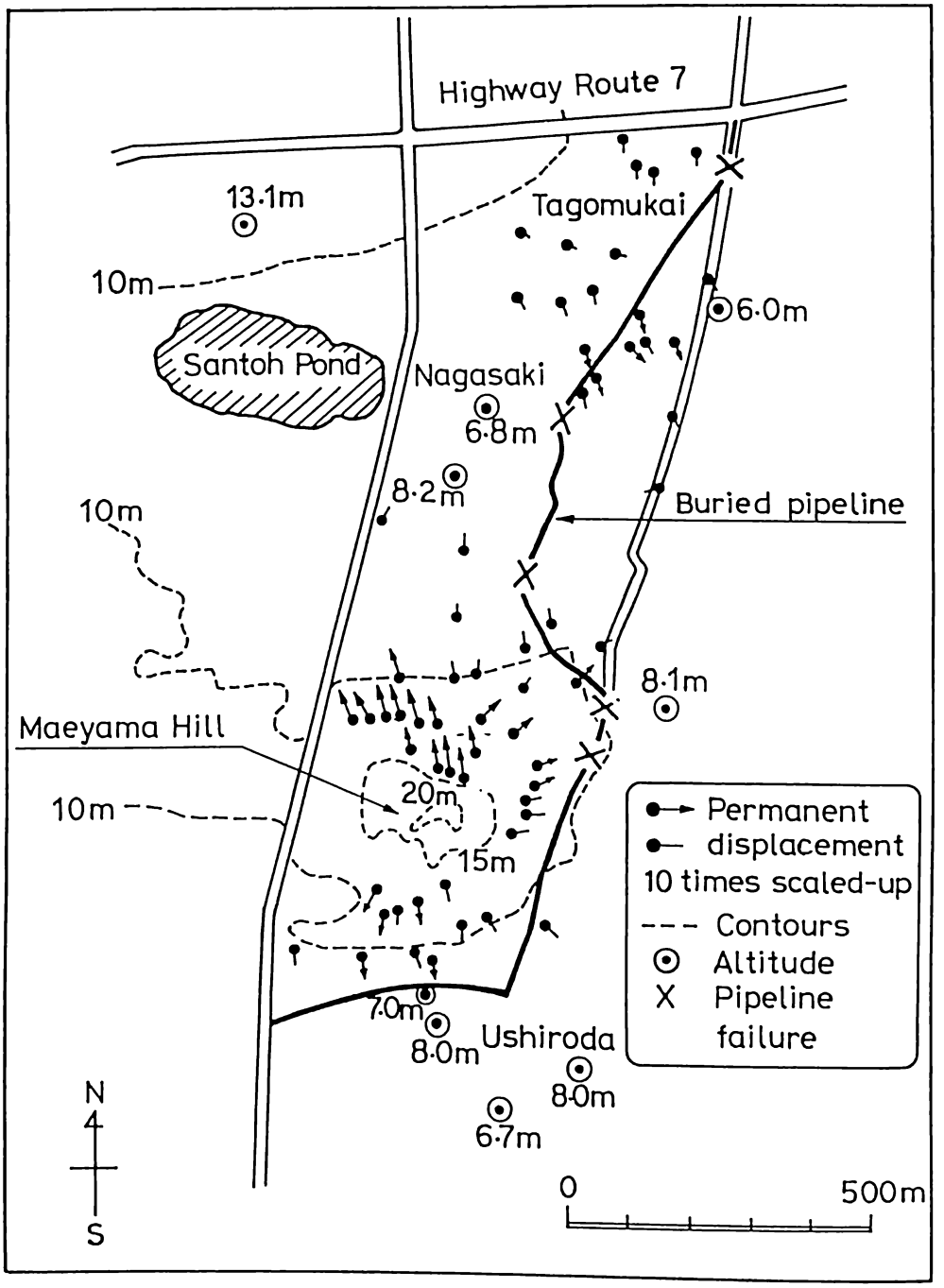

Figure 12: Observed permanent ground displacements in Noshiro City (after Hamada et al., 1986)

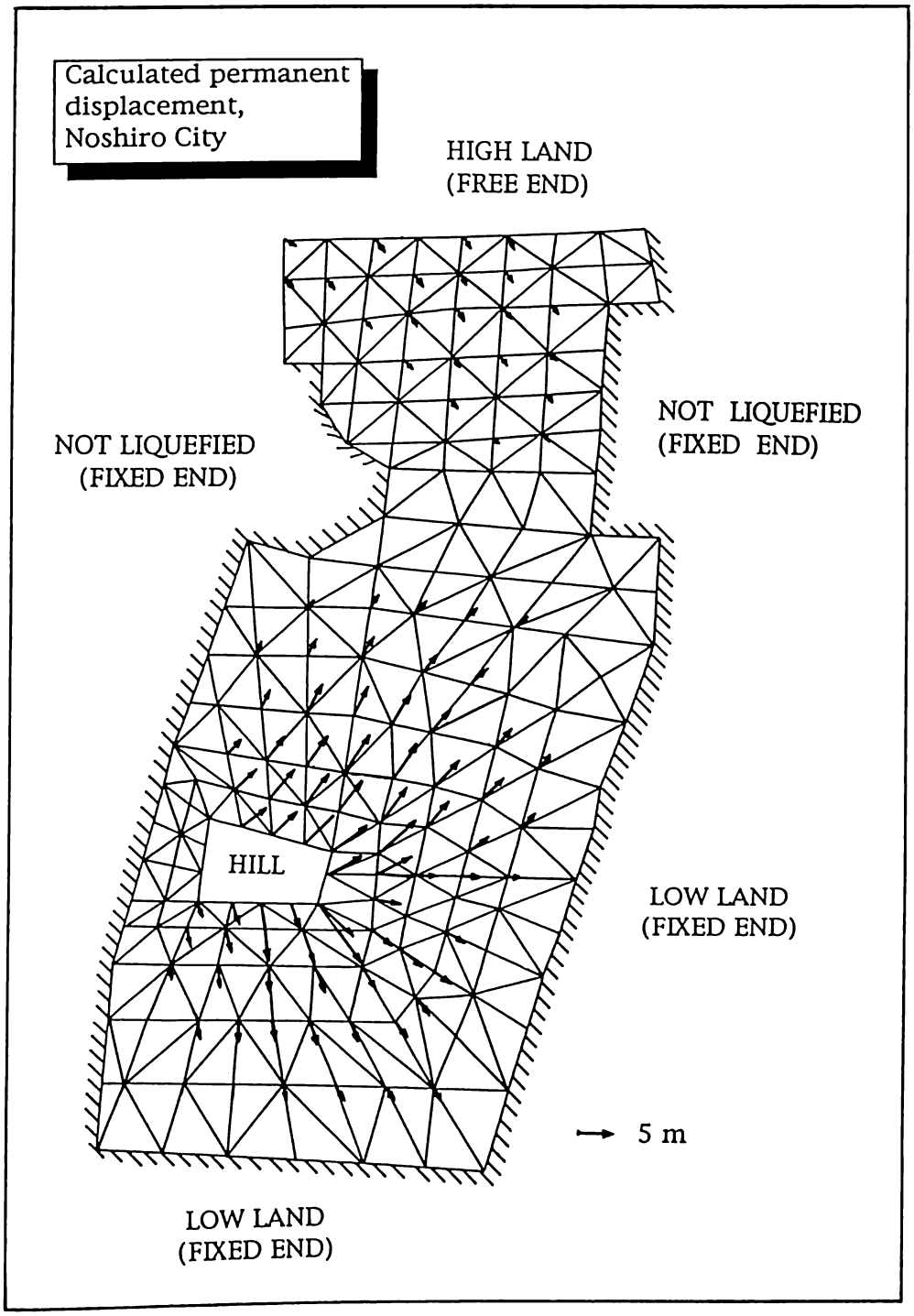

Figure 13: Calculated permanent ground displacements in Noshiro City

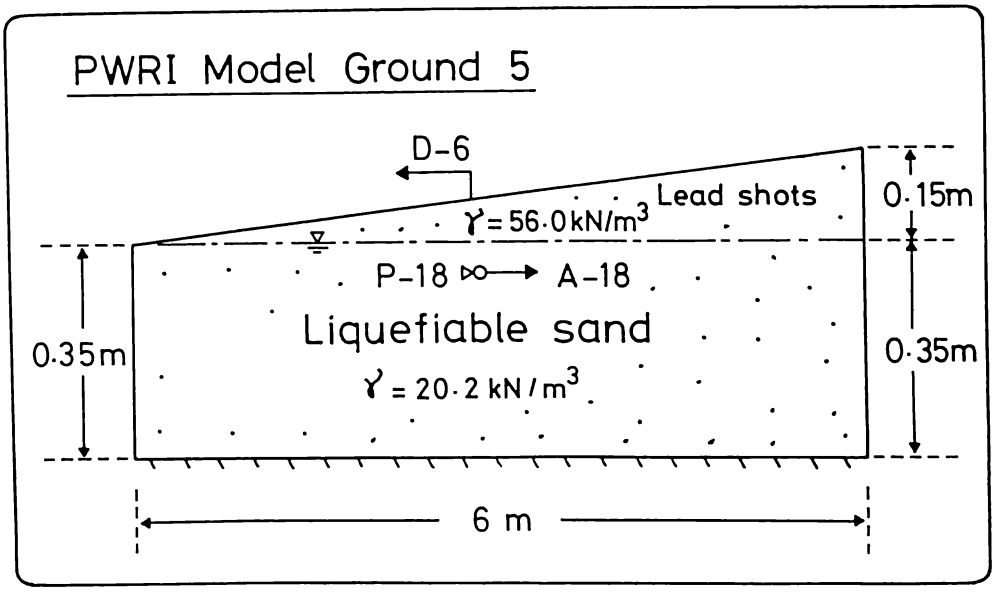

Figure 14: Configuration of model ground in Model 5 test at PWRI

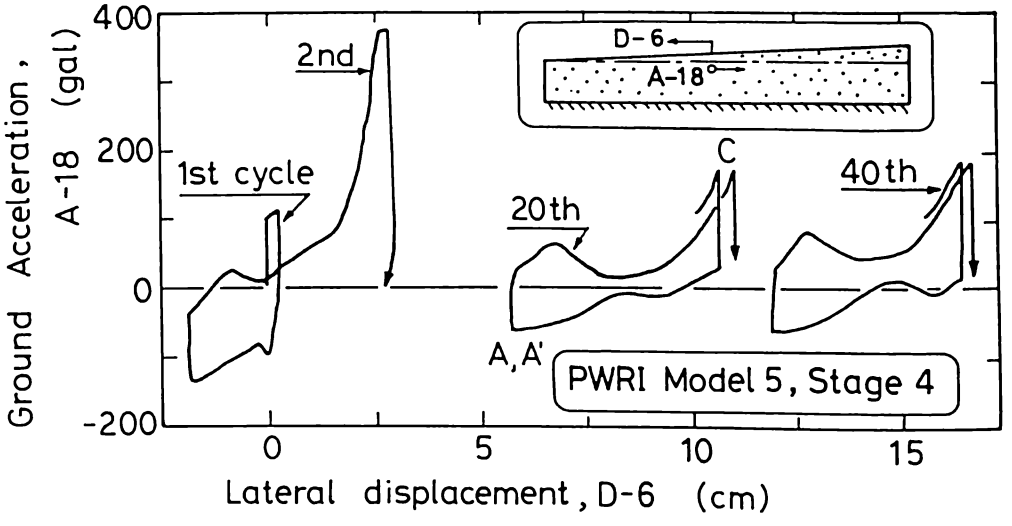

Figure 15: Approximate shape of stress-strain relation of liquefied ground

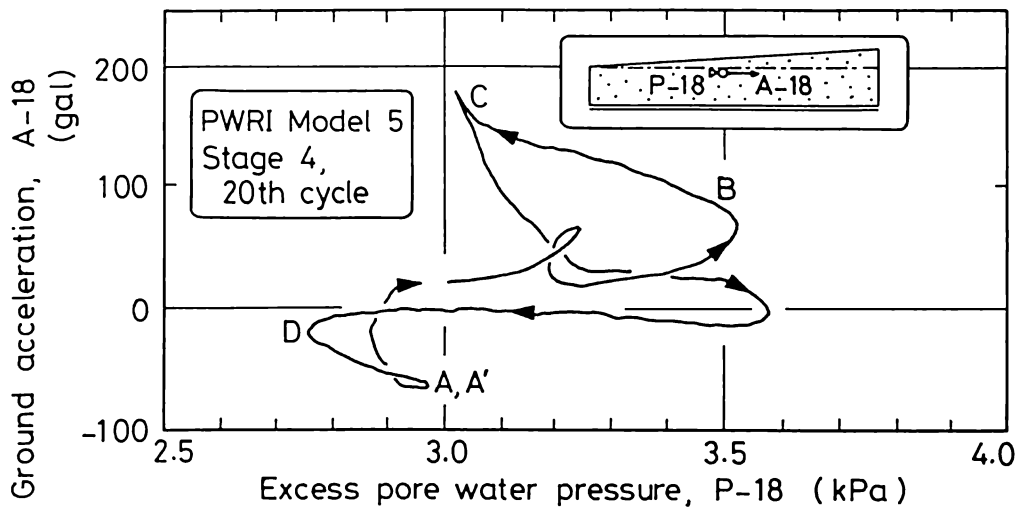

Figure 16: Estimated relationship between pore water pressure and shear stress in liquefied layer

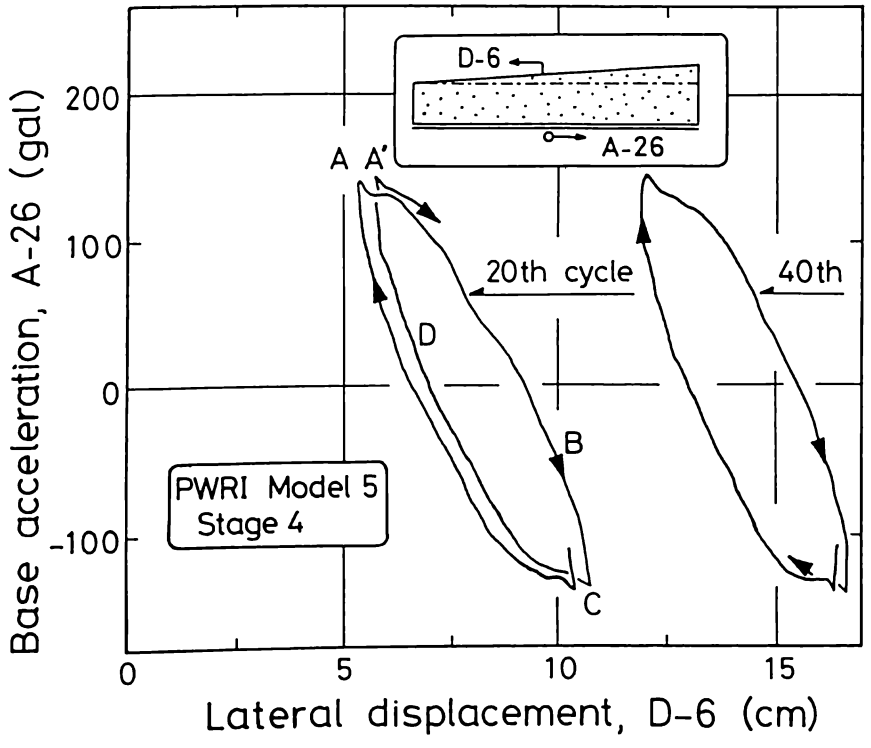

Figure 17: Observed relationship between inertia force and displacement of liquefied ground

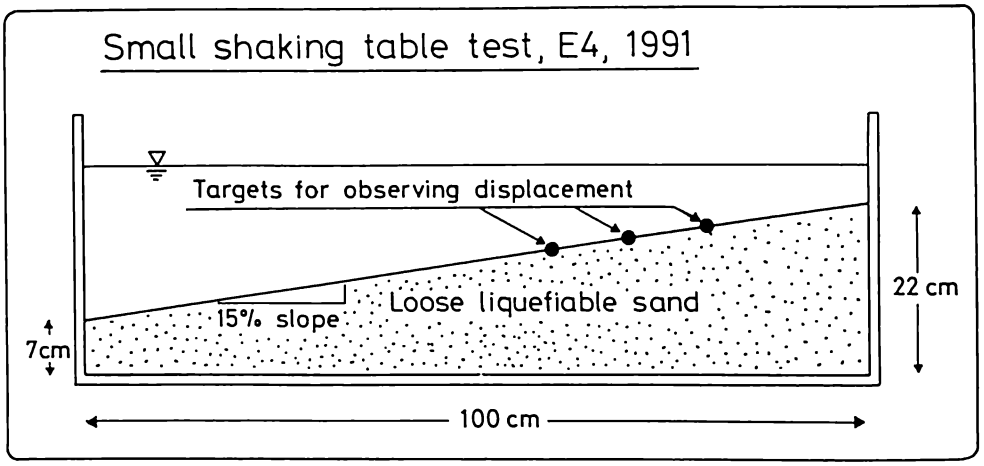

Figure 18: Configuration of model ground E-4

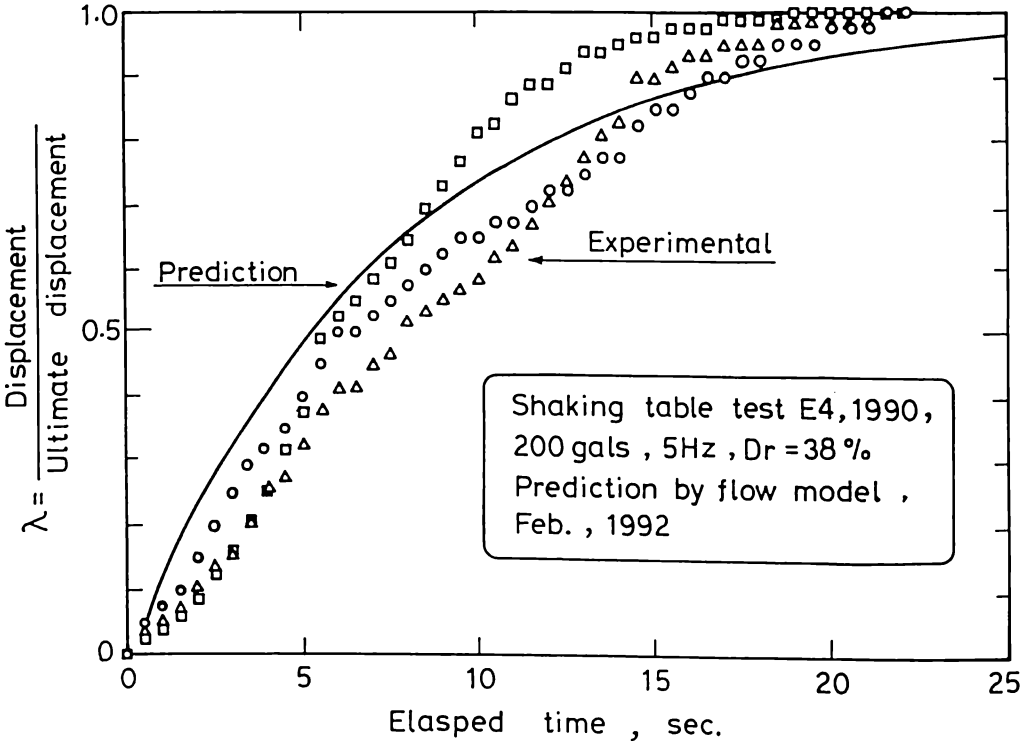

Figure 19: Comparison between the observed and experimental development of λ with time

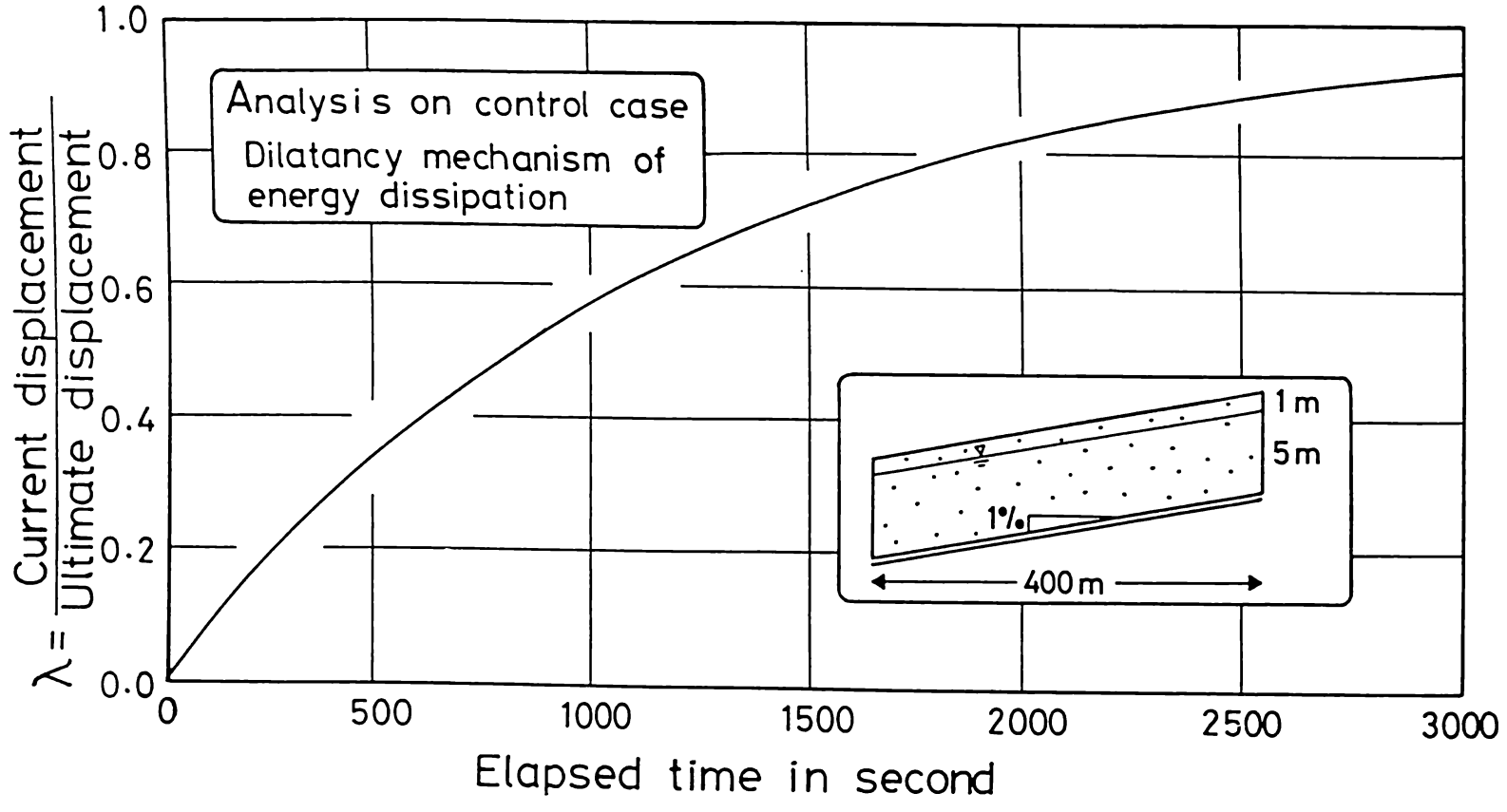

Figure 20: Displacement of a 400 m long ground calculated by the model